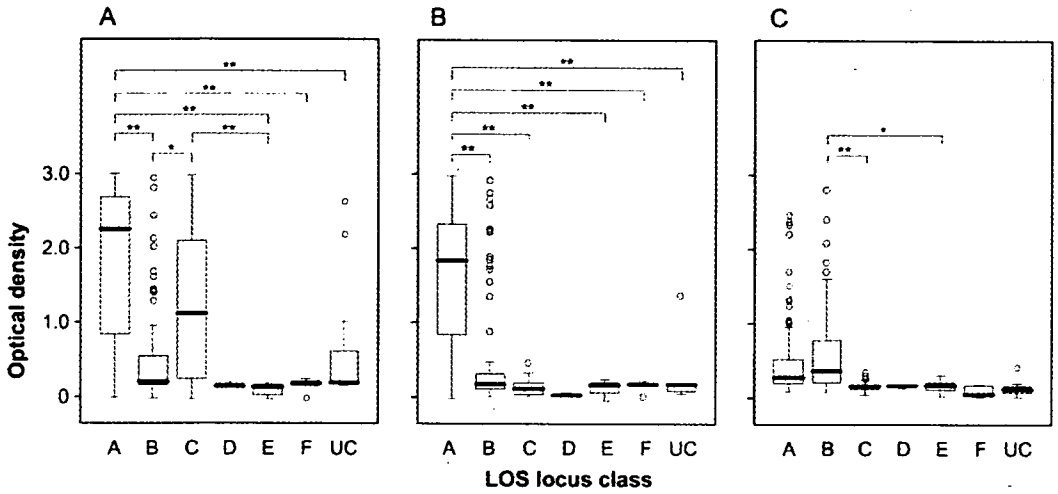

Figure 2. Box and whisker plot of *Campylobacter jejuni* lipo-oligosaccharide reactivity with anti-GM1 (GB2; *A*), anti-GD1a (GB1; *B*), and anti-GQ1b/GT1a (FS3; *C*) monoclonal antibodies in an ELISA. Strains are grouped by lipo-oligosaccharide (LOS) locus class (A–F and unclassified [UC]). Center lines denote medians, boxes denote 25%–75% percentiles, whiskers denote 10% and 90% percentiles, and white circles denote outliers. $^{*}P < .05$; $^{**}P < .01$ (Scheffé's test).

100% identical to the corresponding region in the *C. jejuni* HS:19 type strain (GenBank accession number AF167344), which also expresses a mixture of GM1 and GD1a mimics in its LOS outer core [17].

Risk factors for development of GBS. Because univariate analysis showed that class A strains were associated with GBS, we compared the features of GBS-associated and enteritis-associated class A strains. Differences remained significant between GBS-associated and enteritis-associated strains in the frequency of the HS:19 serotype, the frequency of *cstII* (Thr51), and LOS binding of anti-GM1 and anti-GD1a IgG autoantibodies (table 5). All HS:19 strains with the class A locus had the *cstII* (Thr51) genotype, except for the 2 GBS-associated strains (OH4382 and OH4384) that were obtained from siblings with GBS and external ophthalmoplegia [30]; these 2 strains were known to carry GD3-like or GT1a-like LOSs [17], as well as the GM1 epitope [39], all of which are present with the *cstII* (Asn51) genotype. Multiple logistic regression modeling was used to adjust the comparisons between GBS-associated and enteritis-associated strains for the class A locus, the HS:19 serotype, the *cstII* (Thr51) genotype, and GM1-like and GD1a-like LOSs. In that analysis, the difference remained significant for the HS:19 serotype (odds ratio [OR], 16.5 [95% confidence interval {CI}, 4.0–68.8]; $P < .001$) and the class A locus (OR, 5.6 [95% CI, 2.1–15.1]; $P = .001$).

DISCUSSION

We confirmed the finding of Godschalk et al. [15] that GBS is associated with the class A locus of *C. jejuni* and provided evidence of the first GBS-related *C. jejuni* characteristic that is common to strains from Asia and Europe. Moreover, we found that strains with the class A locus regularly express both the GM1 and the GD1a epitope on their LOSs; this unique LOS profile among *C. jejuni* strains results in an increased risk of producing anti-GM1 and anti-GD1a IgG autoantibodies and, therefore, developing GBS. Expression of the GM1 and GD1a epitopes in class A strains was enhanced in strains that were also serotype HS:19, and this expression was possibly dependent on the predominance of the *cstII* (Thr51) genotype in HS:19 strains. Of course, microbial properties alone do not sufficiently explain why an autoimmune response is triggered in only a minority of individuals with *C. jejuni* enteritis. Host susceptibility must be much more important. Previous attempts to find common host immunogenetic factors in patients with *C. jejuni* GBS, however, have had negative or conflicting results [40–44].

The class A locus is 11.5 kb and has 13 genes. A and B class loci have the same gene profile, except that the class B locus has *orf5II (cgtAII)*, which may be the result of duplication of *orf5I (cgtAI)* [27]. This raises the question as to why GBS-associated strains primarily have the class A locus. Our findings suggest that nucleotide sequence variation within genes is the answer. In fact, strains with the same LOS biosynthesis

Table 4. Lipid A variants and variable terminal sialic acids of an *O*-deacylated sample from *Campylobacter jejuni* strain CF90-26.

The table is available in its entirety in the online edition of the *Journal of Infectious Diseases*.

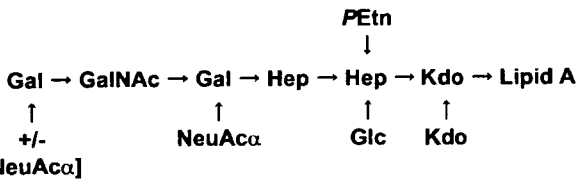

Figure 3. Proposed lipo-oligosaccharide outer core structures as determined on the basis of capillary electrophoresis–electrospray ionization mass spectrometric analysis of *O*-deacylated lipo-oligosaccharide samples from *Campylobacter jejuni* strain CF90-26. Gal, galactose; GalNAc, *N*-acetylgalactosamine; Hep, L-glycero-D-manno-heptose; Glc, glucose; Kdo, 3-deoxy-D-manno-2-octulosonic acid; NeuAc, *N*-acetylneuraminic acid; PEtn, phosphoethanolamine.

gene content have been shown to express diverse ganglioside mimics because of phase variation, a single nucleotide deletion, or single or multiple nucleotide mutations of LOS biosynthesis genes [27]. As we reported in the present study, class A strains regularly had *cstII* (Thr51), which is indicative that this genotype is a feature of class A strains and is related to the onset of GBS, because *cstII* (Thr51) encodes an enzyme with α-2,3-sialyltransferase activity that transfers a single α-2,3-sialic acid to both the inner and the terminal galactose residues, resulting in GM1 and GD1a mimics (figure 1) [27].

Candidate enzyme functions of the class A locus have been proposed, and most of them seem to be essential for the biosynthesis of ganglioside-like LOS [28, 45–47]. This suggests that the content of a single gene of *C. jejuni* is insufficient for the development of GBS; the entire gene content of the class A locus is essential. Nachamkin et al. [19] reported that the 3 glycosyltransferase genes that are necessary for ganglioside-like LOS biosynthesis—*cstII/cstIII* (sialyltransferase), *cgtA* (β-1,4-*N*-acetylgalactosaminyltransferase), and *cgtB* (β-1,3-galactosyltransferase)—[28] are more often present in GBS-associated strains than in enteritis-associated strains. These 3 genes are present in class A, B, and C loci [27], which agrees with our finding that 96% of GBS-associated strains had the class A, B, or C locus. This strongly suggests that the class A, B, or C locus is required to induce the development of GBS, although the class C locus is a much weaker risk factor than is the class A locus.

Interestingly, class A strains regularly express GM1-like and GD1a-like LOSs, whereas class C strains express GM1-like LOS only. GM1 and GD1a are candidate target antigens for the circulating autoantibody [10]. Our results suggest that multiple ganglioside mimicry is more effective for developing GBS than is single ganglioside mimicry. This disagrees with the findings of Nachamkin et al. [19] that the expression of the GD1a epitope alone is associated with GBS. The reason for this discrepancy is not known. We have shown in the present study, however, that patients from whom class A strains were isolated often had both anti-GM1 and anti-GD1a IgG autoantibodies; in addition, the inoculation of rabbits with CF90-26 LOS (which has GM1 and GD1a mimics) caused acute motor axonal neuropathy that was accompanied by anti-GM1 antibodies, not by anti-GD1a antibodies [14]. The assumption that GM1 mimicry, in addition to GD1a mimicry, is responsible for the development of GBS, therefore, is reasonable.

On the basis of chemical analysis, the coexistence of the GM1 and GD1a epitopes on the outer core of the LOS of the HS:19 serotype reference strain has been reported [17]. Elsewhere, we showed by use of mAb immunostaining that both epitopes were present in a GBS-associated HS:19 strain (CF90-26) [38], and we confirmed that finding in the present study by use of mass-spectrometric analysis. Furthermore, the nucleotide sequence of the 6.1-kb PCR product that included *cstII*, *cgtA*, and *cgtB* (as well as downstream and upstream sequences) was identical to the corresponding region in the *C. jejuni* HS:19 type strain that also expresses mixed GM1 and GD1a mimics [17]. This finding confirms that the DNA sequence, as well as

Table 5. Comparison of Guillain-Barré syndrome–associated and enteritis-associated *Campylobacter jejuni* strains with the class A lipo-oligosaccharide (LOS) locus.

Characteristic	Guillain-Barré syndrome–associated strains (n = 72)	Enteritis-associated strains (n = 17)	2-tailed P[a]	OR (95% CI)
Serotype HS:19	66 (92)	6 (35)	<.001	20.2 (5.5–73.9)
cstII polymorphism				
Thr51	66 (92)	10 (58)	.002	7.7 (2.1–27.6)
Asn51	6 (8)	7 (41)	.002	0.13 (0.036–0.47)
Median OD ± SD of mAb to LOS[b]				
GM1-like LOS	2.402 ± 0.897	1.106 ± 1.107	.002	
GD1a-like LOS	1.976 ± 0.830	0.558 ± 1.215	.03	
GQ1b/GT1a-like LOS	0.086 ± 0.431	0.126 ± 0.500	.11	

NOTE. Data are no. (%) of strains, unless otherwise indicated. CI, confidence interval; mAb, monoclonal antibody; OR, odds ratio.

[a] Fisher's exact test or Mann-Whitney *U* test.

[b] ODs were measured by an ELISA with mAbs GB2 (GM1), GB1 (GD1a), and FS3 (GQ1b/GT1a).

the makeup of glycosyltransferase genes, is responsible for determining the type of ganglioside mimic that is formed on LOSs.

In the present study, we found that most of the FS-associated strains had the class A or B locus, which supports the finding of van Belkum et al. [48] that *cstII* was present in all 8 strains with GQ1b-like LOS that they tested. Godschalk et al. [15] found that all 4 of the FS-associated strains that they tested had the class B locus, whereas a significant number of FS-associated strains that we tested in the present study had the class A locus. Furthermore, the differences between the class A and the class B locus were not important in our FS-associated strains, whereas the *cstII* (Asn51) genotype was critical. *cstII* (Asn51) has both α-2,3- and α-2,8-sialyltransferase activities [27], which are essential for transferring the disialyl moiety to the outer core of LOS, thereby mimicking GQ1b and GT1a gangliosides. Our findings suggest that the ganglioside-like LOS synthesis gene contents of *cstII, cgtA,* and *cgtB,* which are common to the class A and B loci, are important for triggering an autoimmune response and that *cstII* polymorphism is the determinant of autoantibody reactivity and neurological presentations in GBS and FS.

Acknowledgments

We thank Maki Okazaki, for her support during the polymerase chain reaction experiment; Denis Brochu, Scott Houliston, Frank St. Michael, and Evgeny Vinogradov, for the lipo-oligosaccharide analyses; Marie-France Karwaski and Sonia Leclerc, for help with the DNA sequencing; and Yukihiro Nishimoto (Department of Pediatrics, Kinan General Hospital, Wakayama, Japan), Takayuki Masaki (Chemo-Sero-Therapeutic Research Institute, Kumamoto, Japan), Shigeru Matsushita (Tama Branch Laboratory, Tokyo Metropolitan Institute of Public Health, Tokyo, Japan), and Maiko Murai (Department of Neurology, Saiseikai Central Hospital, Tokyo, Japan), for providing the *Campylobacter jejuni* strains from patients with enteritis.

References

1. Jacobs BC, Rothbarth PH, van der Meché FGA, et al. The spectrum of antecedent infections in Guillain-Barré syndrome: a case-control study. Neurology **1998**; 51:1110–5.
2. McCarthy N, Giesecke J. Incidence of Guillain-Barré syndrome following infection with *Campylobacter jejuni.* Am J Epidemiol **2001**; 153: 610–4.
3. Kuroki S, Saida T, Nukina M, et al. *Campylobacter jejuni* strains from patients with Guillain-Barré syndrome belong mostly to Penner serogroup 19 and contain β-*N*-acetylglucosamine residues. Ann Neurol **1993**; 33:243–7.
4. Goddard EA, Lastovica AJ, Argent AC. *Campylobacter* O:41 isolation in Guillain-Barré syndrome. Arch Dis Child **1997**; 76:526–8.
5. Takahashi M, Koga M, Yokoyama K, Yuki N. Epidemiology of *Campylobacter jejuni*-isolated Guillain-Barré and Fisher syndromes in Japan. J Clin Microbiol **2005**; 43:335–9.
6. Fisher M. An unusual variant of acute idiopathic polyneuritis: syndrome of ophthalmoplegia, ataxia and areflexia. N Engl J Med **1956**; 255:57–65.
7. Prendergast MM, Moran AP. Lipopolysaccharides in the development of the Guillain-Barré syndrome and Miller Fisher syndrome forms of acute inflammatory peripheral neuropathies. J Endotoxin Res **2000**; 6: 341–59.
8. Rees JH, Soudain SE, Gregson NA, Hughes RAC. *Campylobacter jejuni* infection and Guillain-Barré syndrome. N Engl J Med **1995**; 333: 1374–9.
9. Endtz HP, Ang CW, van den Braak N, et al. Molecular characterization of *Campylobacter jejuni* from patients with Guillain-Barré and Miller Fisher syndromes. J Clin Microbiol **2000**; 38:2297–301.
10. Willison HJ, Yuki N. Peripheral neuropathies and anti-glycolipid antibodies. Brain **2002**; 125:2591–625.
11. Chiba A, Kusunoki S, Obata H, Machinami R, Kanazawa I. Serum anti-GQ1b IgG antibody is associated with ophthalmoplegia in Miller Fisher syndrome and Guillain-Barré syndrome: clinical and immunohistochemical studies. Neurology **1993**; 43:1911–7.
12. Susuki K, Yuki N, Hirata K. Fine specificity of anti-GQ1b IgG and clinical features. J Neurol Sci **2001**; 185:5–9.
13. Goodyear CS, O'Hanlon GM, Plomp JJ, et al. Monoclonal antibodies raised against Guillain-Barré syndrome-associated *Campylobacter jejuni* lipopolysaccharides react with neuronal gangliosides and paralyze muscle-nerve preparations. J Clin Invest **1999**; 104:697–708.
14. Yuki N, Susuki K, Koga M, et al. Carbohydrate mimicry between human ganglioside GM1 and *Campylobacter jejuni* lipo-oligosaccharide causes Guillain-Barré syndrome. Proc Natl Acad Sci USA **2004**; 101: 11404–9.
15. Godschalk PCR, Heikema AP, Gilbert M, et al. The crucial role of *Campylobacter jejuni* genes in autoimmune antibody induction. J Clin Invest **2004**; 114:1659–65.
16. Yuki N, Taki T, Inagaki F, et al. A bacterium lipopolysaccharide that elicits Guillain-Barré syndrome has a GM1 ganglioside-like structure. J Exp Med **1993**; 178:1771–5.
17. Aspinall GO, McDonald AG, Pang H, Kurjanczyk LA, Penner JL. Lipopolysaccharides of *Campylobacter jejuni* serotype O:19 structures of core oligosaccharide regions from the serostrain and two bacterial isolates from patients with Guillain-Barré syndrome. Biochemistry **1994**; 33:241–9.
18. Nam Shin JE, Ackloo S, Mainkar AS, et al. Lipo-oligosaccharides of *Campylobacter jejuni* serotype O:10: structures of core oligosaccharide regions from a bacterial isolate from a patient with the Miller-Fisher syndrome and from the serotype reference strain. Carbohydr Res **1997**; 305:223–32.
19. Nachamkin I, Liu J, Li M, et al. *Campylobacter jejuni* from patients with Guillain-Barré syndrome preferentially expresses a GD1a-like epitope. Infect Immun **2002**; 70:5299–303.
20. Ang CW, Laman JD, Willison HJ, et al. Structure of *Campylobacter jejuni* lipopolysaccharides determines antiganglioside specificity and clinical features of Guillain-Barré and Miller Fisher patients. Infect Immun **2002**; 70:1202–8.
21. Duim B, Ang CW, van Belkum A, et al. Amplified fragment length polymorphism analysis of *Campylobacter jejuni* strains isolated from chickens and from patients with gastroenteritis or Guillain-Barré or Miller Fisher syndromes. Appl Environ Microbiol **2000**; 66:3917–23.
22. Engberg J, Nachamkin I, Fussing V, et al. Absence of clonality of *Campylobacter jejuni* in serotypes other than HS:19 associated with Guillain-Barré syndrome and gastroenteritis. J Infect Dis **2001**; 184:215–20.
23. Nachamkin I, Engberg J, Gutacker M, et al. Molecular population genetic analysis of *Campylobacter jejuni* HS:19 associated with Guillain-Barré syndrome and gastroenteritis. J Infect Dis **2001**; 184:221–6.
24. Leonard EE II, Tompkins LS, Falkow S, Nachamkin I. Comparison of *Campylobacter jejuni* isolates implicated in Guillain-Barré syndrome and strains that cause enteritis by a DNA microarray. Infect Immun **2004**; 72:1199–203.
25. Gilbert M, Godschalk PCR, Parker CT, Endtz HP, Wakarchuk WW. Genetic bases for the variation in the lipooligosaccharide outer core of *Campylobacter jejuni* and possible association of glycosyltransferase genes with post-infectious neuropathies. In: Ketley J, Konkel M, eds.

Campylobacter: molecular and cellular biology. Norwich, UK: Horizon Scientific Press, **2005**:219–48.
26. Parker CT, Horn ST, Gilbert M, Miller WG, Woodward DL, Mandrell RE. Comparison of *Campylobacter jejuni* LOS biosynthesis loci from a variety of sources. J Clin Microbiol **2005**; 43:2771–81.
27. Gilbert M, Karwaski M-F, Bernatchez S, et al. The genetic bases for the variation in the lipo-oligosaccharide of the mucosal pathogen, *Campylobacter jejuni*: biosynthesis of sialylated ganglioside mimics in the core oligosaccharide. J Biol Chem **2002**; 277:327–37.
28. Gilbert M, Brisson J-R, Karwaski M-F, et al. Biosynthesis of ganglioside mimics in *Campylobacter jejuni* OH4384: identification of the glycosyltransferase genes, enzymatic synthesis of model compounds, and characterization of nanomole amounts by 600-MHz ^{1}H and ^{13}C NMR analysis. J Biol Chem **2000**; 275:3896–906.
29. Koga M, Takahashi M, Masuda M, Hirata K, Yuki N. *Campylobacter* gene polymorphism as a determinant of clinical features of Guillain-Barré syndrome. Neurology **2005**; 65:1376–81.
30. Yuki N, Tsujino Y. Familial Guillain-Barré syndrome subsequent to *Campylobacter jejuni* enteritis. J Pediatr **1995**; 126:162.
31. Asbury AK, Cornblath DR. Assessment of current diagnostic criteria for Guillain-Barré syndrome. Ann Neurol **1990**; 27(Suppl): S21–4.
32. Odaka M, Yuki N, Hirata K. Anti-GQ1b IgG antibody syndrome: clinical and immunological range. J Neurol Neurosurg Psychiatry **2001**; 70:50–5.
33. Hitchcock PJ, Brown TM. Morphological heterogeneity among *Salmonella* lipopolysaccharide chemotypes in silver-stained polyacrylamide gels. J Bacteriol **1983**; 154:269–77.
34. Koga M, Gilbert M, Li J, et al. Antecedent infections in Fisher syndrome: a common pathogenesis of molecular mimicry. Neurology **2005**; 64:1605–11.
35. Szymanski CM, St Michael F, Jarrell HC, et al. Detection of conserved *N*-linked glycans and phase-variable lipooligosaccharides and capsules for *Campylobacter* cells by mass spectrometry and high resolution magic angle spinning NMR spectroscopy. J Biol Chem **2003**; 278:24509–20.
36. St Michael F, Szymanski CM, Li J, et al. The structures of the lipo-oligosaccharide and capsule polysaccharide of *Campylobacter jejuni* genome sequenced strain NCTC 11168. Eur J Biochem **2002**; 269: 5119–36.
37. Yuki N, Tagawa Y, Irie F, Hirabayashi Y, Handa S. Close association of Guillain-Barré syndrome with antibodies to minor monosialogangliosides GM1b and GM1α. J Neuroimmunol **1997**; 74:30–4.
38. Yuki N, Taki T, Takahashi M, et al. Penner's serotype 4 of *Campylobacter jejuni* has a lipopolysaccharide that bears a GM1 ganglioside epitope as well as one that bears a GD1a epitope. Infect Immun **1994**; 62:2101–3.
39. Yuki N, Handa S, Tai T, et al. Ganglioside-like epitopes of lipopolysaccharides from *Campylobacter jejuni* (PEN 19) in three isolates from patients with Guillain-Barré syndrome. J Neurol Sci **1995**; 130:112–6.
40. Rees JH, Vaughan RW, Kondeatis E, Hughes RAC. HLA-class II alleles in Guillain-Barré syndrome and Miller Fisher syndrome and their association with preceding *Campylobacter jejuni* infection. J Neuroimmunol **1995**; 62:53–7.
41. Koga M, Yuki N, Kashiwase K, Tadokoro K, Juji T, Hirata K. Guillain-Barré and Fisher's syndromes subsequent to *Campylobacter jejuni* enteritis are associated with HLA-B54 and Cw1 independent of anti-ganglioside antibodies. J Neuroimmunol **1998**; 88:62–6.
42. Magira EE, Papaioakim M, Nachamkin I, et al. Differential distribution of HLA-DQβ/DRβ epitopes in the two forms of Guillain-Barré syndrome, acute motor axonal neuropathy and acute inflammatory demyelinating polyneuropathy (AIDP): identification of DQβ epitopes associated with susceptibility to and protection from AIDP. J Immunol **2003**; 170:3074–80.
43. Ma JJ, Nishimura M, Mine H, et al. HLA and T-cell receptor gene polymorphisms in Guillain-Barré syndrome. Neurology **1998**; 51:379–84.
44. Geleijns K, Jacobs BC, van Rijs W, Tio-Gillen AP, Laman JD, van Doorn PA. Functional polymorphisms in LPS receptors CD14 and TLR4 are not associated with disease susceptibility or *Campylobacter jejuni* infection in Guillain-Barré patients. J Neuroimmunol **2004**; 150:132–8.
45. Guerry P, Ewing CP, Hickey TE, Prendergast MM, Moran AP. Sialylation of lipooligosaccharide cores affects immunogenicity and serum resistance of *Campylobacter jejuni*. Infect Immun **2000**; 68:6656–62.
46. Linton D, Gilbert M, Hitchen PG, et al. Phase variation of a β-1,3 galactosyltransferase involved in generation of the ganglioside GM1-like lipo-oligosaccharide of *Campylobacter jejuni*. Mol Microbiol **2000**; 37: 501–14.
47. Linton D, Karlyshev AV, Hitchen PG, et al. Multiple *N*-acetyl neuraminic acid synthetase *(neuB)* genes in *Campylobacter jejuni*: identification and characterization of the gene involved in sialylation of lipo-oligosaccharide. Mol Microbiol **2000**; 35:1120–34.
48. van Belkum A, van den Braak N, Godschalk P, et al. *Campylobacter jejuni* gene associated with immune-mediated neuropathy. Nat Med **2001**; 7:752–3.

Genetic Dissection of Vasculitis, Myeloperoxidase-Specific Antineutrophil Cytoplasmic Autoantibody Production, and Related Traits in Spontaneous Crescentic Glomerulonephritis-Forming/Kinjoh Mice[1]

Yoshitomo Hamano,[2]* Kazuyuki Tsukamoto,* Masaaki Abe,* Guo Dong Sun,* Danqing Zhang,* Hiroaki Fujii,* Shuji Matsuoka,* Masumi Tanaka,* Akiko Ishida-Okawara,† Hitoshi Tachikawa,† Hiroyuki Nishimura,‡ Kazuhiro Tokunaka,§ Sachiko Hirose,* and Kazuo Suzuki†

The spontaneous crescentic glomerulonephritis-forming/Kinjoh (SCG/Kj) mouse is a model of human crescentic glomerulonephritis and vasculitis associated with the production of the myeloperoxidase (MPO)-specific antineutrophil cytoplasmic autoantibody (MPO-ANCA). Although the disease is mediated initially by mutation of the *Fas* gene (*lpr*), SCG/Kj mice also have non-*Fas* predisposing genetic factors. To define these factors, genome-wide quantitative trait locus (QTL) mapping was performed on female (B_6× SCG/Kj) F_2 intercross mice. Fourteen non-*Fas* QTLs were identified. QTLs of glomerulonephritis were located on chromosomes 1, 10, 13, 16, and 17, vasculitis on chromosomes 1 and 17, splenomegaly on chromosome 1, hypergammaglobulinemia on chromosomes 1, 2, 4, 6, 7, 11, 13, and 17, antinuclear Ab on chromosomes 1, 8, 10, and 12, and MPO-ANCA production on chromosomes 1 and 10. Significant QTLs derived from SCG/Kj on chromosomes 1, 2, 7, and 13 were designated *Scg-1* to *Scg-5*, respectively, and those derived from B_6 on chromosomes 4, 6, 17, and 10 were designated *Sxb-1* to *Sxb-4*, respectively. Two loci linked to MPO-ANCA production on chromosomes 1 and 10 were designated *Man-1* and *Man-2* (for MPO-ANCA), respectively. Although both *Scg-1* and *Scg-2* were on chromosome 1 and shared several functions, it was of interest that aberrant MPO-ANCA production was exclusively controlled by *Man-1*, the centromeric half region of the *Scg-2* chromosomal segment. We also examined the epistatic effects between the *lpr* mutation and non-*Fas* susceptibility genes. QTLs are discussed in relation to previously described loci, with emphasis on their candidate genes. ***The Journal of Immunology*****, 2006, 176: 3662–3673.**

The spontaneous crescentic glomerulonephritis (CrGN)[3]-forming/Kinjoh (SCG/Kj) mouse has been described as an animal model of rapidly progressive CrGN and systemic vasculitis (1). This strain consists of recombinant inbred mice derived from (BXSB/Mp × MRL/Mp-*lpr/lpr*) F_2 and is characterized by early development of nephritis and systemic vasculitis. The characteristics of renal histology are extreme formation of crescents in most of Bowman's capsules with diffuse endocapillary and mesangial proliferation (1, 2). Vasculitis occurs in multiple organs, including kidney, ovary, uterus, spleen, heart, and stomach (1).

The primary immunological defects responsible for the initiation and progression of disease in SCG/Kj mice are unclear. Recent studies show that the antineutrophil cytoplasmic autoantibody (ANCA) is associated with both CrGN and small-vessel vasculitis, and myeloperoxidase (MPO)-specific ANCA (MPO-ANCA) is particularly important for pathogenesis of pauci-immune vasculitis and glomerulonephritis (GN) (3). Our previous study has demonstrated that aberrant MPO-ANCA production and consequent hyperfunction of neutrophils are involved in the manifestation of CrGN and vasculitis in SCG/Kj mice (4). However, genetic predisposition, the key element in susceptibility, remains to be understood. Several mouse models of autoimmune diseases, such as systemic lupus erythematosus (SLE), have collectively contributed toward understanding the disease and have led to the definition of susceptible quantitative trait loci (QTLs) (5–7).

In this study, we identified QTLs susceptible for GN, crescent formation, vasculitis, and the production of autoantibodies, including MPO-ANCA, by establishing (B_6× SCG/Kj) F_2 intercross mice. Using a genome-wide scan, we found multiple QTLs from both parental strains that predispose to disease, including aberrant production of MPO-ANCA.

Materials and Methods

Mice

Female C57BL/6 (B_6) mice were purchased from the Shizuoka Laboratory Animal Center. Male SCG/Kj mice were bred and maintained at the animal

*Department of Pathology, Juntendo University School of Medicine, Bunkyo-ku, Tokyo, Japan; †Biodefense Laboratory, National Institute of Infectious Diseases, Shinjuku-ku, Tokyo, Japan; ‡Toin Human Science and Technology Center, Department of Biomedical Engineering, Toin University of Yokohama, Yokohama-shi, Kanagawa, Japan; and §Nippon Kayaku Co., Ltd., Kita-ku, Tokyo, Japan

Received for publication August 2, 2005. Accepted for publication January 3, 2006.

The costs of publication of this article were defrayed in part by the payment of page charges. This article must therefore be hereby marked *advertisement* in accordance with 18 U.S.C. Section 1734 solely to indicate this fact.

[1] This work was supported in part by a grant for the Special Study Group on Progressive Glomerular Disease from the Ministry of Health, Labor, and Welfare of Japan.

[2] Address correspondence and reprint requests to Dr. Yoshitomo Hamano, Department of Pathology, Juntendo University School of Medicine, 2-1-1 Hongo, Bunkyo-ku, Tokyo 113-8421, Japan. E-mail address: hamanoyoshitomo@jcom.home.ne.jp

[3] Abbreviations used in this paper: CrGN, crescentic glomerulonephritis; ANCA, antineutrophil cytoplasmic autoantibody; BSF1, (B_6× SCG/Kj) F_1; BSF2, (B_6× SCG/Kj) F_2; BUN, blood urea nitrogen; DAF, decay-accelerating factor; GN, glomerulonephritis; LOD, logarithm of odds; MPO, myeloperoxidase; MPO-ANCA, MPO-specific ANCA; NZB, New Zealand Black; NZW, New Zealand White; PAI-2, plasminogen activator inhibitor type 2; QTL(s), quantitative trait locus (loci); SCG/Kj, spontaneous crescentic glomerulonephritis-forming/Kinjoh; SLE, systemic lupus erythematosus.

0022-1767/06/$02.00

facility of Nippon Kayaku under specific pathogen-free conditions. Female B_6 and male SCG/Kj were crossed to obtain (B_6× SCG/Kj) F_1 (BSF1) mice, and brother-sister mating of F_1 produced a total of 420 female (B_6× SCG/Kj) F_2 (BSF2) animals. These F_1 and F_2 mice, as well as parental strains, were maintained in our own animal facility. Only female mice were investigated. All procedures were approved by the Juntendo University Subcommittee on Animal Research (Tokyo, Japan), and the animal care methods and experimental protocols were based on the guidelines for animal experiments set by the National Institute of Infectious Diseases (Tokyo, Japan).

Sample collection and measurement of blood urea nitrogen (BUN) and proteinuria

Peripheral blood was obtained from periorbital sinus. The white blood cell count was done by the MEK-6158 automatic blood cell counter (Nihon Koden). Urine was tested for proteinuria biweekly as described by Knight et al. (8) with minor modifications. BUN was measured by a kit using the urease-indophenol method (Wako Junyaku). Hematuria was tested with Uropaper II urine dipsticks (Eiken Kagaku). Serum collection was done at 12 and 24 wk of age, except for the SCG/Kj mice. Because severe CrGN was manifested in most of the female SCG/Kj mice, who died at 12–16 wk of age, their sera at 24 wk of age were not taken. Mice were sacrificed at 24 wk of age or when proteinuria was >200 mg/dl and hematuria was >20 RBC/μl (1+).

ELISA for serum autoantibody and total Ig levels

Serum levels of total Ig and IgG-class autoantibodies to DNA and chromatin were determined by ELISA. Ninety-six-well flat-bottom plates (Immulon 2; Dynatech Laboratories) were coated with 0.001% protamine sulfate followed by DNA or chromatin. dsDNA was obtained by digestion of calf thymus DNA (Sigma-Aldrich) with S1 nuclease (Seikagaku Kogyo), followed by fractionation on a hydroxylapatite column. ssDNA was obtained by heat denaturation of calf thymus DNA. Chromatin was prepared as described (9). Briefly, nucleosomes were isolated by solubilizing chromatin from purified chicken erythrocyte nuclei with micrococcal nuclease. The solubilized chromatin was fractionated into sucrose gradients that were analyzed for monomers using electrophoresis, and the appropriated fractions were dialyzed and pooled. To measure the amount of immunoglobulins, plates were coated with goat anti-mouse IgM or IgG Abs. Wells were blocked by 50% FCS for 1 h. After washing, the diluted sera were applied to the plates. After a 1-h incubation at room temperature, plates were washed in PBS with 0.05% Tween 20. After washing, appropriately diluted peroxidase-conjugated goat anti-mouse γ Abs were added. The preparations were then incubated for 1 h at room temperature and washed, and the substrate (*o*-phenylenediamine dihydrochloride) diluted in 0.1 M citrate phosphate buffer (pH 5.0) with 0.5 μg/mg H_2O_2 was added. The reaction was stopped by adding 2.5 N H_2SO_4, and the OD was measured at 490 nm using a microplate reader (Viento; Dainippon Pharmaceutical). The DNA- and chromatin-binding activities were expressed in units referring to a standard curve obtained by serial dilutions of a standard serum pool from 7- to 9-mo-old (New Zealand Black (NZB) × New Zealand White (NZW)) F_1 mice containing 1000 U/ml. The amounts of total IgM and IgG were calculated using a standard curve obtained by affinity-purified serum IgM and IgG derived from (NZB × NZW) F_1 mice.

ELISA for measurement of MPO-ANCA

MPO-ANCA levels were measured as described (4). Briefly, recombinant mouse MPO was coated onto an ELISA plate (TS plate; Toyoshima) overnight at 4°C. The plate was blocked, and mouse serum (×50 dilution) was added for 1.5 h at room temperature. Alkaline phosphatase-labeled anti-mouse IgG Ab (×1000 dilution) was added and allowed to react for 2 h at room temperature. Afterward, *p*-nitrophenyl phosphate as the alkaline phosphatase substrate was added at a concentration of 1 mg/ml and incubation at room temperature, the absorbance at 405 nm was measured by a model LFA-096 automatic analyzer (Jasco). The titer of MPO-ANCA in mouse sera was described as rabbit anti-mouse MPO IgG (μg/ml).

Histopathology

At autopsy, the spleen was weighed and the kidneys were fixed in 10% formalin in 0.01 mol/L phosphate buffer (pH 7.2) and embedded in paraffin. They were stained with H&E and periodic acid-Schiff for histopathological examinations by light microscopy.

Kidneys from one individual were dissected into more than four sections. Four independent kidney sections were observed, and 30 glomeruli in each section were evaluated so that 120 glomeruli were examined for one individual. Among these, 20 glomeruli with both vascular and tubular poles were evaluated for endocapillary and mesangial proliferative lesions and sclerotic lesions of mesangial areas. The trait for GN was expressed as the percentage of glomeruli with more than one of the following three glomerular lesions: endocapillary proliferation, mesangial proliferation, and mesangial sclerosis.

The trait for crescentic formation was expressed as numbers of glomeruli with cellular and/or fibrous crescents among 120 glomeruli. Vasculitis was expressed as numbers of small vessels with granulomatous vasculitis in four independent kidney sections. Granulomatous vasculitis in this study is defined as vascular lesions with at least one of following findings: perivascular infiltration of lymphocytes, destruction of the vascular wall, and/or myointimal thickening of the vascular wall.

Microsatellite genotyping

Genotypes were determined by PCR using selected simple sequence length polymorphism markers purchased from either Research Genetics or Invitrogen Life Technologies. *D19MIT87* was used for the genotyping of the *Fas* gene, because it was located within 1 cM of chromosome 19 in the mouse genome database consensus map (The Jackson Laboratory; http://www.informatics.jax.org). Genotyping for the polymorphic FcγRIIB promoter region was done by PCR using a previously described primer pair (10). Genomic DNA of mice were extracted from tail samples stored at −70. Primers flanking chromosomal microsatellite markers (forward primer labeled on the 5′ end with the fluorescent dyes FAM, VIC, PET, or NED and reverse primers) were purchased from Applied Biosystems. A PCR mixture (7 μl) contained 110 nM each primer, 0.23 mM each dNTP, 16 mM Tris-HCl (pH 8.3), 41 mM KCl, 2.7 mM $MgCl_2$, 2.0 μg/ml genomic DNA, and 0.03 U/μl *Taq* polymerase (Invitrogen Life Technologies). The PCR mixtures were distributed on MicroAmp optical 96-well reaction plates (Applied Biosystems) using a PT-100 Molecular Biology Station (System Biotics), and amplifications were conducted using PCR System 9700 thermal cyclers (Applied Biosystems). The reaction consisted of initial denaturation at 92°C for 5 min followed by 35 cycles of 92°C for 1 min, 56–58°C for 1.5 min, and 72°C for 2 min, and final incubation at 72°C for 7 min. PCR products were analyzed using an Applied Biosystems 3100 genetic analyzer and genotyped with GENESCAN and GENOTYPER software (Applied Biosystems).

Statistical analyses

Comparison of renal function (BUN), serum levels of IgM and IgG class immunoglobulins, serum levels of IgG-class autoantibodies (anti-ssDNA, anti-dsDNA and antichromatin antibodies), MPO-ANCA, three histopathological traits in kidneys and spleen weight, and survival weeks among strains were performed with the Mann-Whitney *U* test or ANOVA. Associations between traits in F_2 mice were determined by correlation coefficients with *p* values derived from Fisher's transformation. For detection of QTLs for crescent formation, χ^2 tests were conducted. In χ^2 tests, F_2 progenies that had more than three glomeruli with crescents were regarded as positive. All analyses were performed using StatView, version 4.0 (Abacus Concepts) or Microsoft Excel.

Linkage analyses and interval mappings

The linkage map for the BSF2 intercross was created using MapManager QTX (Dr. K. F. Manly, University of Tennessee Health Science Center (Memphis, TN); http://www.mapmanager.org/mmQTX.html). Interval mapping for QTL detection was done by MapManager QTX in a free regression model. Likelihood ratio statistics were converted to conventional base-10 logarithm of odds (LOD) scores. To establish suggestive and significant threshold values, permutation tests were performed using MapManager QTX as previously described (11) with 1000 permutations of the data. Only loci with suggestive or significant linkages were shown in the figures and tables, and only those that were significant were named.

Results

Disease traits in SCG/Kj, B_6, F_1, and F_2 intercross mice

As summarized in Table I, parental SCG/Kj and B_6 mice, as well as BSF1 and BSF2 mice, were examined for levels of BUN as a marker of renal function and autoantibodies at 12 and 24 wk of age. SCG/Kj presented significantly higher levels of total IgM and IgG class Ig ($p < 0.05$ and $p < 0.0001$, respectively), anti-ssDNA Ab ($p < 0.0001$), anti-dsDNA Ab ($p < 0.0001$), antichromatin Ab ($p < 0.0001$), and MPO-ANCA ($p < 0.0001$) than B_6 at 12 wk of age. Although comparison of BUN between these two parental strains was not significant, marked renal dysfunction (127 mg/dl in

Table I. *Renal function and serological findings*[a]

Mice	BUN	Total IgM	Total IgG	ssDNA	dsDNA	Chromatin	MPO-ANCA
12 wk old							
B_6	26.1 ± 0.8	38.0 ± 4.8	4.6 ± 0.4	22.6 ± 3.8	13.5 ± 0.7	6.7 ± 4.1	22.6 ± 15.5
SCG/Kj	37.4 ± 12.9	66.0 ± 9.2	42.2 ± 7.5	2943 ± 532	2179 ± 671	304 ± 107	2250 ± 861
BSF1	31.2 ± 0.9	62.0 ± 4.9	8.9 ± 0.4	136 ± 27	42.2 ± 11	11.6 ± 5.8	85.8 ± 66.5
BSF2	30.5 ± 0.9	109.9 ± 7.1	21.5 ± 1.6	603 ± 57	331 ± 44	62.2 ± 12	1603 ± 379
24 wk old[b]							
B_6	25.0 ± 0.9	66.7 ± 9.8	6.3 ± 0.49	39.7 ± 9.1	14.9 ± 1.1	4.7 ± 1.5	49.3 ± 47
BSF1	29.6 ± 1.8	119 ± 12	16.0 ± 2.2	811 ± 359	399 ± 180	317 ± 118	550 ± 184
BSF2	30.9 ± 0.6	175 ± 9.7	32.0 ± 2.4	1035 ± 77	644 ± 62	229 ± 31	5939 ± 903

[a] Mean ± SEM values are shown for BUN (mg/dl), total IgM and IgG (μg/ml), anti-dsDNA, ssDNA and chromatin Ab (ELISA unit/ml), and MPO-ANCA (μg/ml).
[b] SCG/Kj mice were not examined at 24 wk (see *Materials and Methods*).

BUN) was already observed in one SCG/Kj individual that was not observed in B_6 mice until the end of experiment. Levels of total IgG, anti-ssDNA Abs, and anti-dsDNA Abs were significantly higher in BSF1 mice than in B_6 mice (in all comparisons, $p < 0.005$), but these levels in BSF1 mice were much lower than those in SCG/Kj mice. Mean levels of antichromatin Ab and MPO-ANCA were higher in BSF1 mice than in B_6 mice but not significant. As for total IgM, the level was slightly lower in BSF1 mice than in SCG/Kj mice but was not significant. These facts suggest that the mode of inheritance of Ig and autoantibody production is incomplete dominance with dominance effects of various degrees.

Kidneys of each strain were evaluated in terms of endocapillary and mesangial proliferation, mesangial sclerosis, crescent formation, and vasculitis. Endocapillary and mesangial proliferation and mesangial sclerosis were recognized as findings of GN; GN and crescent formation were regarded as independent traits. Crescent formation was expressed as number of glomeruli with cellular and/or fibrous crescent because this trait had less penetrance than GN. As summarized in Table II, GN findings were manifested in 12 of 13 (92%) individuals of SCG/Kj mice, and mean glomeruli with GN amounted to 62.3% of total glomeruli in one individual. Kidneys of B_6 mice presented virtually no GN findings ($p < 0.0001$). There was a tendency for the kidneys of F_1 mice to present more severe GN and more crescents than those of B_6 mice, but the degree was about one-third of that of SCG/Kj. These facts suggest that the mode of inheritance of GN and crescent formation is incomplete dominance, as seen in autoantibody production.

Histopathological findings of vasculitis in SCG/Kj, BSF1, and BSF2 mice were all similar to that of MRL/*lpr*. As described in the studies of Nose et al. (12), vasculitis in these strains was characterized by granulomatous changes with marked perivascular infiltration of lymphocytes, destruction of external lamina, and myointimal thickening of vascular wall. It has been pointed out (6) that the grading systems for evaluation of murine vasculitis are not ideal parameters in QTL analyses, even after conversion to various mathematical functions. For better suitability as a variate for QTL analyses, we expressed vasculitis as the number of inflammatory lesions observed in four independent kidney sections. Twenty small vessels were observed in each of four sections for a total of 80 vessels in a single individual. The mean value of vasculitis in SCG/Kj was significantly higher than that in B_6 mice ($p < 0.0001$). Vasculitis in BSF1 mice was significantly more severe than in B_6 mice ($p < 0.05$) but much less severe than in SCG/Kj mice. Again, this finding indicates that vasculitis is inherited in the mode of incomplete dominance.

Spleen weight seemed to be inherited in the same mode as other traits. Spleens were significantly heavier in SCG/Kj and BSF1 than in B_6 mice ($p < 0.0001$ and $p < 0.01$, respectively), but spleen weights in BSF1 were about one-third of those in SCG/Kj mice ($p < 0.0001$).

Disease traits in BSF2 mice were distributed in a wide range and were generally between parental extremes. A minority of BSF2 mice exhibited trait values outside parental ranges. Presumably, this resulted from the recombination of genetic components in F_2 mice, that is, the inheritance of unique combinations of SCG/Kj and B_6 alleles.

Correlation between serological and histopathological traits in BSF2 mice

In BSF2 mice, serological and histopathological traits were statistically examined by association study. Histopathological traits were also tested to elucidate correlations (Table III). All Ig and autoantibody levels were significantly ($p < 0.005$) correlated with histopathological traits, with a positive correlation coefficient (r) ranging from 0.139 to 0.617 (data not shown). MPO-ANCA, considered one of the major causal factors for pathogenesis of human polyarteritis and pauci-immune-type CrGN (3), significantly correlated with crescent formation ($r = 0.159$). MPO-ANCA exhibited better correlation with vasculitis ($r = 0.413$).

Table II. *Histological findings in kidneys and splenomegaly*[a]

Mice (n)	Proliferative and Sclerotic Lesions (GN)[b]	Crescent Formation[c]	Renal Vasculitis[d]	Spleen Weight (grams)
B_6 (14)	0.39 ± 0.39	0 ± 0	0.077 ± 0.077	0.099 ± 0.006
SCG/Kj (13)	62.3 ± 7.86	20.3 ± 10.2	14.6 ± 1.84	0.851 ± 0.044
BSF1 (14)	14.6 ± 9.15	1.57 ± 1.57	2.93 ± 1.11	0.393 ± 0.093
BSF2 (383)	26.8 ± 1.80	2.96 ± 0.63	3.60 ± 0.31	0.322 ± 0.017

[a] Mean ± SEM values are shown for all traits.
[b] Percentage of glomeruli with endocapillary/mesangial proliferative and/or sclerotic lesions.
[c] Number of glomeruli with cellular and/or fibrous crescents among 120 glomeruli.
[d] Number of small vessels with at least one of the following findings: perivascular infiltration of lymphocytes, destruction of the vascular wall, and myointimal thickening of the vascular wall.

Table III. *Strength of association among MPO-ANCA, histopathological traits and lifespan in BSF2 mice*[a]

Traits	Age (wk)	Proliferative and Sclerotic Lesions (GN)	Crescent Formation	Renal Vasculitis	Lifespan
MPO-ANCA	12	0.308[b]	0.139[c]	0.172[d]	−0.271[b]
	24	0.359[b]	0.159[c]	0.413[b]	−0.321[b]
Proliferative and sclerotic lesions (GN)			0.445[b]	0.628[b]	−0.564[b]
Crescent		0.445[b]		0.403[b]	−0.601[b]
Renal vasculitis		0.628[b]	0.403[b]		−0.401[b]

[a] Strength of association expressed as Pearson's correlation coefficient (r) and p values.
[b] $p < 0.0001$.
[c] $p = 0.0037$.
[d] $p = 0.003$.
[e] $p = 0.0008$.

Correlations among three histopathological traits were all statistically significant ($p < 0.0001$). All correlation coefficients were >0.403. GN and vasculitis correlated most strongly ($r = 0.628$) among all association studies. Correlations between crescent and GN and between crescent and vasculitis were less strong (r = 0.445 and 0.403, respectively).

Survival of mice was expressed as total lifespan by the week. All five serological traits, as well as three histopathological ones, significantly correlated with lifespan ($p < 0.0001$ for all correlations, $r = -0.187$ to -601; Table III and data not shown). The trait that exhibited the strongest negative correlation with lifespan among histopathological traits was crescent formation ($r = -0.601$).

Mapping panel and subcohorts according to the genotype of the Fas gene

We genotyped 420 BSF2 intercross mice to identify QTLs contributing to disease phenotypes. All intercross mice analyzed were female. Seven hundred twenty-seven microsatellite markers were analyzed for size polymorphism between B_6 and SCG/Kj mice, and 158 markers were informative (21.1% of total markers). A total of 102 polymorphic microsatellite markers were used to construct a linkage map designed to cover the whole mouse autosomal genome. Because of a failure in some cases to identify informative markers, gaps of >20 cM were present in four chromosomal regions. These four gaps were located on chromosome 7 between *D7MIT80* and *D7MIT207* with a distance of 20 cM, on chromosome 9 between *D9MIT42* and *D9MIT53* with a distance of 29 cM, on chromosome 14 between the centromere and *D14MIT5* with a distance of 21.7 cM, and on chromosome 15 between *D15MIT26* and *D15MIT15* with a distance of 21.5 cM. Two hundred seventy-two markers were investigated to shorten these four and other minor gaps, but they were all noninformative. As a result, markers were distributed throughout the autosomes such that 85% of the genome was within 20 cM of an informative marker. The low frequency of informative markers in BSF2 is probably because SCG/Kj originated from crossing BXSB and MRL/*lpr* (1). Because ~50% of the BXSB genome (13) is from B_6 mice, markers on such a common chromosomal segment are expected to be nonpolymorphic.

We observed that the *Fas* locus on chromosome 19 was the major gene controlling all disease phenotypes (range of LOD from 9.7 for 12-wk MPO-ANCA to 105.0 for 24-wk ssDNA Ab, and range of percentage variance from 11% for 12-wk antichromatin Ab to 70% for 24-wk anti-ssDNA Ab; Table IV). In these analyses, mice homozygous for the *lpr* alleles of the *Fas* gene (*lpr/lpr*) exhibited much higher or more severe traits compared with those of mice heterozygous (+/*lpr*) or homozygous for the B_6 alleles (+/+). Several traits were revealed to be significantly higher in mice heterozygous for *Fas* than in mice homozygous for the B_6 alleles ($p < 0.05$ for the 12-wk anti-dsDNA Ab level; $p < 0.005$ for the 12-wk and 24-wk total IgM and 24-wk anti-dsDNA Ab levels; and $p < 0.0005$ for the 24-wk total IgG and 24-wk MPO-ANCA levels and splenomegaly). These facts suggest that the *lpr* mutation of the *Fas* is not completely recessive; therefore, we subdivided the BSF2 mice into seven "*Fas* cohorts" according to the *Fas* genotypes and their combination (Table V). As shown in Table V, the cohort symbolized by S consists of F_2 individuals homozygous for alleles from SCG/Kj (*lpr/lpr*). The B cohort consists of F_2 individuals homozygous for alleles from $\underline{B}_6$ (+/+). The F cohort consists of F_2 individuals heterozygous for B_6 and SCG/Kj alleles (+/*lpr*), the same *Fas* genotype as (B_6× SCG/Kj) $\underline{F}_1$. Cohorts symbolized as SF, BF, and SB (Table V) are those in which two of the three cohorts above are combined, and the SFB cohort consists of all F_2 individuals. The practical meanings of the subcohorts are as follows. First, because cohorts are based on the alleles of the *Fas* gene, QTLs that demonstrate some of the epistatic effects with certain genotype(s) of *Fas* will be revealed in specific *Fas* cohort(s). Second, combined cohorts lead to be a sort of "extreme-phenotype analysis" (14) and are good for discovering minor QTLs. Third, combined cohorts possibly have better resolution and power for finding minor QTLs because they contain more progenies.

Two distinct multifunctional QTLs on chromosome 1

There were two multifunctional QTLs on chromosome 1. As shown in Table IV and Fig. 1, one of these QTLs was the region between *D1MIT11* and *D1MIT102* (an interval of ~14 cM, the position represented by *D1MIT191*), and the other was the region between *D1MIT14* and *D1MIT166* (an interval of 18 cM, the position represented by *D1MIT15*).

The distal QTL on chromosome 1 adjacent to *D1MIT15* exhibited significant linkage to the 12-wk total IgG level, the 12-wk anti-ssDNA Ab production, the 12-wk anti-dsDNA Ab production, and the shortened lifespan in the S cohort (QTL exhibited LOD of 4.4–6.5 and accounted for 16–22% of the variance). This QTL was also significantly linked to the 24-wk total IgG level, the 12-wk antichromatin Ab level, GN, vasculitis, and splenomegaly in the BF cohort (LOD of 3.5–7.0 and 5–20% of the variance). This area on chromosome 1 is designated *Scg-1*; it also exhibited

Table IV. *Phenotypes of BSF2 mice based on significant and suggestive QTLs*

					SFB Cohort[c]		Cohort with Maximum LOD[d]			
Traits (age in wks)	Chromosome	cM[a]	Markers	Allele[b]	LOD	Variance (%)	Cohort	LOD	Threshold values[e]	No Variance (%)
Total IgM (12)	4	61.9	*D4MIT71*	*bb*	1.4	2	BF	5.7	3.6	8
	6	3.5	*D6MIT88*	*bb*	1.6	2	F	3.4	3.5	7
	7	18	*D7MIT80*	*ss*	0.6	1	F	5.4	3.5	11
	13	35	*D13MIT13*	*ss*	3.7	4	S	4.8	3.3	17
	19	23	*Fas*	*ss*	29.2	28	SFB	29.2	3.5	28
Total IgM (24)	4	61.9	*D4MIT71*	*bb*	2.9	3	BF	6.8	3.5	10
	13	35	*D13MIT13*	*ss*	5.5	6	S	6.7	3.5	27
	19	23	*Fas*	*ss*	27.2	28	SFB	27.2	3.5	28
Total IgG (12)	1	63.1	*D1MIT191*	*ss*	4	4	SB	5	3.6	11
		87.9	*D1MIT15*	*ss*	4.3	5	S	6.4	3.7	22
	6	3.5	*D6MIT88*	*bb*	1.5	2	F	4.6	3.5	9
	11	65	*D11MIT58*	*ss*	0.9	1	B	2.8	3.7	15
	17	22.8	*D17MIT64*	*bb*	2.1	2	BF	5.8	3.4	8
	19	23	*Fas*	*ss*	47.7	41	SFB	47.7	3.5	41
Total IgG (24)	1	87.9	*D1MIT15*	*ss*	0.5	1	BF	4.1	3.5	20
	2	84	*D2MIT26*	*ss*	0.8	1	F	4.8	3.5	10
	13	16	*D13MIT60*	*ss*	0.7	1	BF	4.4	3.5	6
	17	18.6	*D17MIT21*	*bb*	1.3	1	BF	5.5	3.5	8
	19	23	*Fas*	*ss*	53.7	46	SFB	53.7	3.6	46
ssDNA Ab (12)	1	63.1	*D1MIT191*	*ss*	4.2	5	SB	4.8	3.7	11
		87.9	*D1MIT15*	*ss*	3.8	4	S	6.5	3.6	22
	10	21	*D10MIT3*	*bs*	3.6	4	SB	4.5	3.7	10
	19	23	*Fas*	*ss*	56.4	46	SFB	56.4	3.5	46
ssDNA Ab (24)	1	100	*D1MIT166*	*ss*	1	1	S	2.9	3.6	13
	10	21	*D10MIT3*	*bs*	1.7	2	SB	3.8	3.6	9
	19	23	*Fas*	*ss*	105	70	SFB	105	3.5	70
dsDNA Ab (12)	1	63.1	*D1MIT191*	*ss*	5.3	6	SB	6.1	3.6	13
		87.9	*D1MIT15*	*ss*	3.6	4	S	4.4	3.5	16
	19	23	*Fas*	*ss*	28.5	27	SFB	28.5	3.5	27
dsDNA Ab (24)	1	100	*D1MIT166*	*ss*	0.9	1	S	2.8	3.5	12
	19	23	*Fas*	*ss*	65.3	53	SFB	65.3	3.5	53
Chromatin Ab (12)	1	87.9	*D1MIT15*	*ss*	2.6	3	BF	3.5	3.5	5
	8	18	*D8MIT189*	*ss*	2.8	3	S	3.5	3.5	13
	19	23	*Fas*	*ss*	10.3	11	SFB	10.3	3.4	11
Chromatin Ab (24)	1	87.9	*D1MIT15*	*ss*	1.7	2	B	2.9	4.1	15
	12	38	*D12MIT214*	*bb*	1.1	1	BF	3.1	3.4	5
	19	23	*Fas*	*ss*	13.2	14	SFB	13.2	3.5	14
MPO-ANCA (12)	1	63.1	*D1MIT191*	*ss*	5.3	6	SB	6	3.9	13
	19	23	*Fas*	*ss*	9.7	45	SFB	9.7	3.7	45
MPO-ANCA (24)	10	21	*D10MIT3*	*bs*	2.9	3	SB	3.6	3.6	9
	19	23	*Fas*	*ss*	30.2	30	SFB	30.2	3.5	30
Proliferative and sclerotic lesions (GN)	1	73	*D1MIT102*	*ss*	2.8	3	BF	3.4	3.6	5
		87.9	*D1MIT15*	*ss*	4.8	6	BF	7	3.6	10
	10	21	*D10MIT3*	*bs*	2.2	3	SB	3.2	3.7	8
	13	10	*D13MIT135*	*ss*	1.5	2	BF	3	3.6	4
	16	27.3	*D16MIT4*	*ss, bs*	1.6	2	SB	3.9	3.7	10
	17	29.5	*D17MIT88*	*bb*	2.3	3	F	2.9	3.5	8
	19	23	*Fas*	*ss*	31.7	33	SFB	31.7	3.4	33
Crescent	19	23	*Fas*	*ss*	11.8	14	SFB	11.8	3.6	14
Vasculitis	1	92.3	*Fcgr2b*	*ss*	1.8	2	BF	3.8	3.5	6
	17	18.6	*D17MIT21*	*bs*	1	1	BF	3.2	3.5	5
	19	23	*Fas*	*ss*	24.2	26	SFB	24.2	3.5	26
Splenomegaly	1	63.1	*D1MIT191*	*ss*	1.9	2	B	4.6	3.8	23
		87.9	*D1MIT15*	*ss*	1.6	2	BF	6.1	3.5	9
	19	23	*Fas*	*ss*	29.6	30	SFB	29.6	3.5	30
Lifespan	1	63.1	*D1MIT191*	*ss*	2.4	3	S	3.2	3.6	12
		87.9	*D1MIT15*	*ss*	3.4	4	S	5.4	3.6	19
		100	*D1MIT166*	*ss*	3.4	4	S	6	3.6	21
	19	23	*Fas*	*ss*	42.5	37	SFB	42.5	3.4	37

[a] Chromosome and cM location from the mouse genome database (http://www.informatics.jax.org).

[b] Genotypes of mice: *s* = SCG/Kj; *b* = B_6.

[c] Results of QTL analysis in all F_2 progenies (SFB cohort). Base-10 LOD score and percentage of trait variance are calculated by MapManager QTX in the free regression model. SFB and other cohorts are defined in Table V

[d] Name of *Fas* cohort in which maximum LOD was observed. LOD score, threshold values, and percent of trait variance in that cohort (free regression model) are also shown.

[e] Significant LOD threshold values by permutation tests. Suggestive LOD threshold values ranged from 1.9 to 2.1 (not shown).

Table V. *Subcohorts of BSF2 mice according to the genotype of the Fas gene (Fas cohorts)*

Symbols of Cohorts	Population	No. of Mice
SFB	All BSF2 progenies	420
S	Progenies with *Fas lpr/lpr*	119
F	Progenies with *Fas* +/*lpr*	219
B	Progenies with *Fas* +/+	82
SF	S plus F	338
BF	B plus F	301
SB	S plus B	201

suggestive linkage to the 24-wk anti-ssDNA Ab level, the 24-wk anti-dsDNA Ab level, and the 24-wk antichromatin level. These traits were all significantly more severe in mice homozygous for the *D1MIT15* allele from SCG/Kj, but mice with heterozygous alleles also exhibited significantly stronger traits than mice homozygous for the allele from B_6 (Fig. 2, *D* and *F*, and data not shown), meaning that this QTL is from SCG/Kj and its effect is additive. Because interval mapping analyses did not identify any QTLs for crescent formation other than the *Fas* gene, we tried χ^2 analysis to find loci for the crescent. In the S cohort, F_2 individuals that had more than three crescents in their kidneys were defined as positive for crescent formation. χ^2 tests for independence on the contingency table by crescent formation and genotypes of markers on the whole genome were performed. As a result, a suggestive or significant linkage to crescent formation was observed at *D1MIT15* (χ^2 = 18.9; $p = 7.7 \times 10^{-5}$) on chromosome 1 (Table VI).

The second QTL that controlled traits including the aberrant production of MPO-ANCA was on the middle of chromosome 1 around *D1MIT191*, 25 cM from *D1MIT15*. This QTL was significantly linked to the 12-wk total IgG level, 12-wk anti-ssDNA Ab production, 12-wk anti-dsDNA Ab production, and 12-wk MPO-ANCA production in the SB cohort (LOD of 4.8–6.1 and 11–13% of the variance). It also presented significant linkage to splenomegaly in the B cohort (LOD of 4.6 and 23% of the variance). Suggestive linkage to GN and lifespan was also observed. This area on chromosome 1 was designated *Scg-2*. A one-log support interval was determined based on the likelihood of 12-wk anti-ssDNA Ab. It is noteworthy that splenomegaly presented significant linkage to *Scg-2* in the cohort without the $Fas^{lpr/lpr}$ or $Fas^{+/lpr}$ individual (B cohort), suggesting that *Scg-2* exerted some effect, if only partial, independently of the *Fas* gene. Although *Scg-1* and *Scg-2* were both multifunctional genes with partially common functions, their spectra of effects were different in the following way: *Scg-1* was suggested as influencing the antichromatin Ab level, vasculitis, and crescent formation, but these traits were not linked to *Scg-2* even at suggestive levels. More surprisingly, the production of MPO-ANCA at 12 wk of age was exclusively controlled by *Scg-2* (Fig. 1*A*). The 12-wk MPO-ANCA presented significant linkage to *Scg-2* in the SFB, S, and SF cohorts, as well as in the SB cohort, but did not present even suggestive linkage to *Scg-1* in any of these cohorts. A genome-wide scan did not identify any significant QTLs predisposing 12-wk MPO-ANCA except *Fas* and *Scg-2*. These facts suggest that *Scg-1* and *Scg-2* are different genes, although both are on chromosome 1. A one-log support interval of MPO-ANCA analysis defined about one-half of the *Scg-2* interval, designated *Man-1* from MPO-ANCA. *Scg-2* was inherited from SCG/Kj. *Scg-2* was inherited recessively, because mice with the *ss* genotype for *D1MIT191* exhibited much stronger

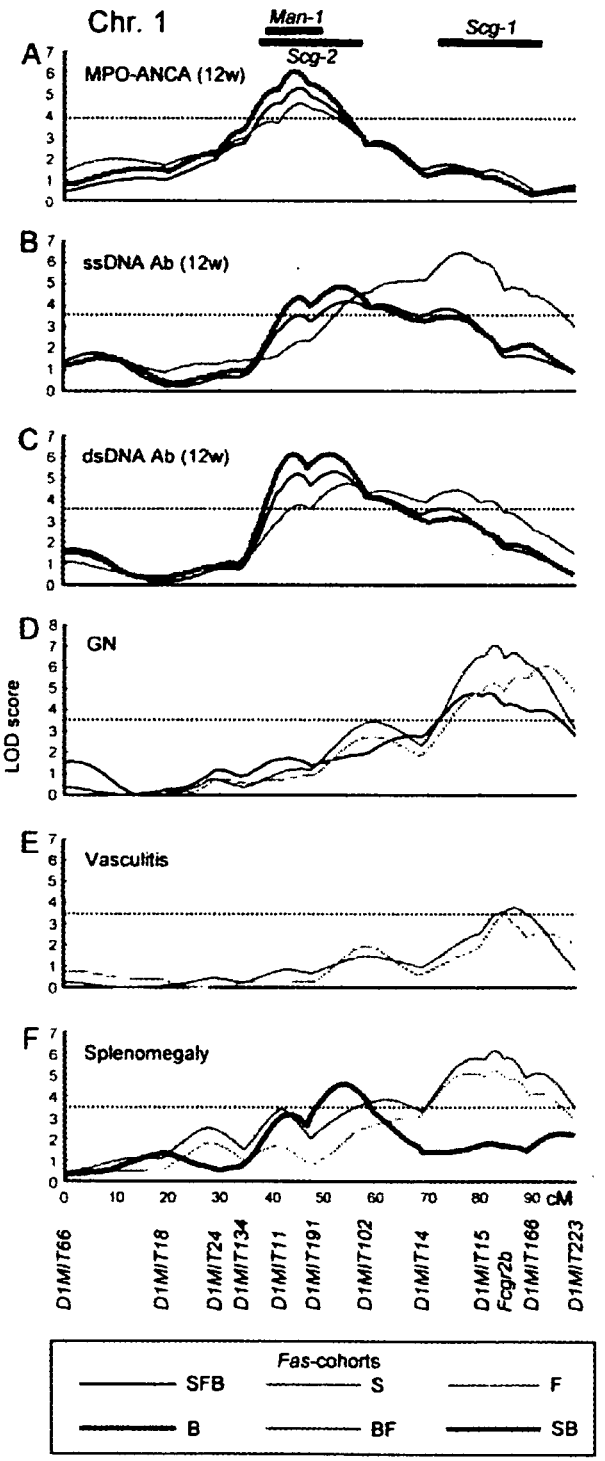

FIGURE 1. Interval mapping scans showing QTLs *Scg-1*, *Scg-2*, and *Man-1* on chromosome 1 (Chr. 1). LOD score curves for each quantitative trait, including MPO-ANCA (*A*), ssDNA Ab (*B*), dsDNA Ab (*C*), GN (*D*), vasculitis (*E*), and splenomegaly (*F*), are shown. The distances between markers (indicated in cM) were generated by MapManager QTX using the Kosambi function. The colors of the lines represent *Fas*-cohorts in which QTL analyses were done. The corresponding cohort and line are shown at the *bottom*. Dotted horizontal lines indicate significant LOD threshold values determined by permutation tests. A one-log support interval for anti-ssDNA Ab is shown with a solid bar at the *top* to define *Scg-1* (*B*). One-log support intervals for anti-dsDNA Ab (*C*) and MPO-ANCA (*A*) are shown to define *Scg-2* and *Man-1*, respectively. 12w, 12-wk-old mice.

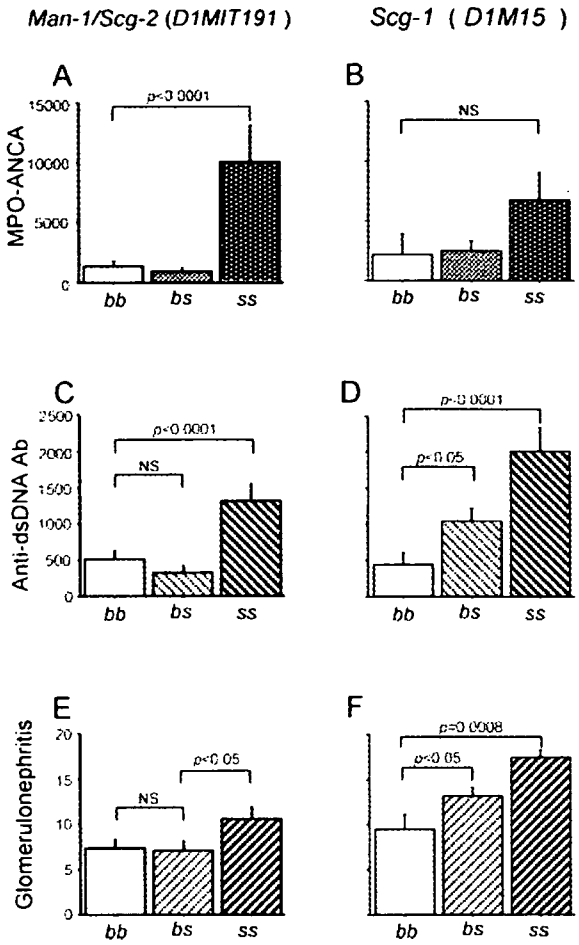

FIGURE 2. Comparison between *Man-1/Scg-2* and *Scg-1*. Differences in MPO-ANCA level (*A* and *B*), anti-dsDNA Ab (*C* and *D*), and GN (*E* and *F*) are shown. F_2 progenies grouped according to genotypes of *D1MIT191* (*Man-1/Scg-2*) and *D1MIT15* (*Scg-1*) were compared using ANOVA. *p* values in Fisher's protected least significant difference procedure are shown. NS, not significant.

traits than those of the *bs* or *bb* genotypes. This result is shown in Fig. 2*A* for the 12-wk MPO-ANCA level and is also the case for the 12-wk total IgG, the 12-wk ssDNA Ab and 12-wk dsDNA Ab levels, and GN (Fig. 2, *C* and *E*, and data not shown). The difference in modes of inheritance also supports the notion that *Scg-1* and *Scg-2* are distinct.

QTLs predisposing to hyperproduction of IgM- and IgG-class immunoglobulins on other chromosomes

Seven to eight non-*Fas* QTLs were identified for aberrant production of IgM- and/or IgG-class immunoglobulins on chromosomes other than chromosome 1 (chromosomes 2, 4, 6, 7, 11, 13, and 17; Table IV). Loci on chromosomes 6 and 13 were linked to the hyperproduction of both IgM and IgG, and the rest were linked to that of either IgM or IgG.

One significant interval, linked to the 24-wk total IgG level, was identified on chromosome 2 between *D2MIT26* and *D2MIT213* (LOD of 4.8 in the F cohort). It was derived from SCG/Kj, accounted for 10% of the variance (Table IV), and was designated *Scg-3* (Fig. 3*A*). The mode of inheritance of *Scg-3* appeared to be recessive (Fig. 4*A*).

Total IgM levels at 12 and 24 wk of age were significantly linked to the telomeric region on chromosome 4 in the BF cohort (LOD of 5.7–6.8 and 8–10% of the variance; Table IV). A broad area distal to *D4MIT178* exhibited a significant level of LOD score, with a peak LOD score at *D4MIT71*, the most telomeric marker in this study (Fig. 3*B*). This area is designated *Sxb-1* (SCG/Kj cross B_6-1), inherited from B_6 (Table IV). It is noteworthy that *Sxb-1* was associated only to IgM-class Ig levels but not to IgG class levels or to specific autoantibody levels. As shown in Fig. 4*B*, *Sxb-1* was additively inherited.

On chromosome 6 there was an area of suggestive linkage (LOD of 3.4 in the F cohort) to the 12-wk total IgM level and an area of significant linkage (LOD of 4.6 in the F cohort) to the 12-wk total IgG level (Table IV and Fig. 3*C*). The patterns of LOD curves for these traits were similar, suggesting that the QTL was identical for each. It was from B_6 and accounted for 7 and 9% of variances of total IgM and IgG, respectively. The area from *D6MIT88* to *D6MIT16* is designated *Sxb-2* (Fig. 3*C*). *Sxb-2* inherited additively (Fig. 4*C*).

The 12-wk total IgM levels were significantly (LOD of 5.4 in the F cohort) linked to a SCG/Kj-derived QTL on mid-proximal chromosome 7 (designated *Scg-4*; Table IV and Fig. 3*D*), accounting for 11% of the variance. The mode of inheritance appeared to be recessive (Fig. 4*D*).

On the mid-proximal region of chromosome 13 (Table IV and Fig. 3*F*) there was an interval that significantly linked the12-wk total IgM level (LOD of 4.8 and 17% of the variance in the S cohort), the 24-wk total IgM level (LOD of 6.7 and 27% of the variance in the S cohort), and the 24-wk total IgG level (LOD of 4.4 and 6% of the variance in the BF cohort). This was a SCG/Kj-derived recessive QTL (Fig. 4*F*). Values of the LOD score over a significant level ranged widely from *D13MIT60* to *D13MIT144*, an interval of ~32 cM (designated *Scg-5*; Fig. 3*F*).

On chromosome 17, significant linkages to 12-wk total IgG (LOD of 5.8 and 8% of the variance in the BF cohort) and 24-wk total IgG (LOD of 5.5 and 8% of the variance in the BF cohort) were observed for the region adjacent to the *H2* gene, a murine MHC (Fig. 3*G*). *D17MIT21*, located between *H2-K* and *H2-A*, represented this region. F_2 progenies with *bb* and *bs* genotypes for *D17MIT21* exhibited significantly higher levels of 12- and 24-wk total IgG than those of mice with the *ss* genotype. This is compatible with the dominant mode of inheritance (Fig. 4*H*). The region around *D17MIT21* is designated *Sxb-3* (Fig. 3*G*).

One minor QTL of suggestive linkage to the 12-wk total IgG level was detected on chromosome 11 around *D11MIT58* (Table IV). It was from SCG/Kj and was inherited in an additive manner (data not shown).

QTLs predisposing autoantibody production and histopathological traits

QTLs for aberrant production of autoantibodies and histopathological phenotypes were searched on the genomes, except chromosomes 1 and 19. On chromosome 10 there was an interesting QTL that controlled the production of anti-ssDNA Ab, MPO-ANCA, and the manifestation of GN. Significant linkages were shown for 12- and 24-wk anti-ssDNA Ab (LOD of 3.8–4.5 and 9–10% of the variance in the SB cohort; Table IV and Fig. 3*E*) and for the 24-wk MPO-ANCA level (LOD of 3.6 and 9% of the variance in the SB cohort; Table IV and Fig. 3*E*). Suggestive linkage was also observed for GN (LOD of 3.2 and 8% of the variance in the SB cohort). All of these traits shared their patterns of LOD curves, and peaks of LOD curves coincided at the position adjacent to *D10MIT3* (Fig. 3*E*). All linkages were observed in the SB cohort, suggesting that this QTL needs the *lpr/lpr* allele of the *Fas* gene for its exertion. Intriguingly, F_2 mice with the *bs* genotype for *D10MIT3* presented stronger traits than mice with *ss* or *bb*. This

Table VI. *QTLs on chromosome 1 linked with crescent formation in S (Fas lpr/lpr) cohort*

Markers	Position (cM)[a]	Crescent Formation: Positive *bb*[b]	Positive *bs*	Positive *ss*	Negative *bb*	Negative *bs*	Negative *ss*	χ^2	*P*
D1MIT66	9	5	25	4	17	24	7	5.14	0.076
D1MIT18	29.7	7	16	11	19	21	9	3.83	0.15
D1MIT24	41	7	15	12	23	16	10	6.24	0.04
D1MIT134	49	6	15	14	22	17	10	7.82	0.02
D1MIT11	58.7	7	14	14	24	15	10	7.91	0.02
D1MIT191	63.1	12	9	13	27	13	9	4.67	0.09
D1MIT102	73	12	11	11	21	21	7	3.88	0.14
D1MIT14	81.6	10	11	14	23	19	7	7.46	0.024
D1MIT15	87.9	3	20	12	20	27	2	18.9	7.7×10^{-5}
Fcgr2b	92.3	5	18	11	20	27	2	14.8	0.0006
D1MIT166	100	3	19	13	20	26	3	18.1	0.0001
D1MIT223	106.3	7	16	11	18	26	5	6.99	0.03

[a] Map position (cM) is based on the mouse genome database.
[b] Genotype of mice: *s* = SCG/Kj and *b* = B_6.

was the case for all three traits, so that some epistatic effect was suggested between SCG/Kj and the B_6 alleles of this QTL (Fig. 4*E*). The region around *D10MIT3* is designated *Sxb-4* and *Man-2*, because it is one of only two non-*Fas* QTLs for MPO-ANCA production.

A QTL for vasculitis was identified on chromosome 17 (*D17MIT21*; LOD of 3.2 and 5% of the variance in the BF cohort), encompassing a region overlapping *Sxb-3*. As opposed to serological traits, F_2 mice with *bs* genotype for *D17MIT21* were most severe in vasculitis (Fig. 4*G*). Another QTL for GN was around *D17MIT88* (LOD of 2.9 in the F cohort), ~11 cM distal to *D17MIT21*. This QTL was derived from B_6 and appeared to be inherited additively (data not shown).

Two loci associated with antichromatin Ab production were identified on chromosomes 8 and 12. The chromosome 8 locus mapped to the mid-proximal portion around *D8MIT189* and was linked to 12-wk antichromatin Ab (LOD of 3.5 and 13% of the variance in S cohort; Table IV). The susceptible allele was inherited from SCG/Kj in a recessive manner (data not shown). Another QTL of possible association with 24-wk antichromatin Ab production (LOD of 3.1 and 5% of the variance in the BF cohort; Table IV) was detected on mid-chromosome 12 around *D12MIT214*. This QTL was from B_6 and was inherited recessively (data not shown).

For GN, a locus of significant linkage was mapped to mid-chromosome 16 (*D16MIT4*; LOD of 3.9 and 10% of the variance in the SB cohort). Because the *ss* and *bs* genotypes equally conferred higher susceptibility to the GN than the *bb* genotype, the pathological allele was derived from SCG/Kj in a dominant manner (data not shown).

Discussion

In this study, we used a panel of (B_6 × SCG/Kj) F_2 intercross mice to define non-Fas^{lpr} susceptibility loci for hypergammaglobulinemia, the aberrant production of autoantibodies including MPO-ANCA, GN, vasculitis, splenomegaly, and shortened lifespan. Fourteen to fifteen QTLs were linked to those traits. Ten significant QTLs were identified on chromosomes 1, 2, 4, 6, 7, 10, 13, 16, and 17. Susceptibility loci inherited from SCG/Kj mice were designated *Scg-1* to *Scg-5*, and loci inherited from B_6 mice were designated *Sxb-1* to *Sxb-4*. Two loci on chromosomes 1 and 10 predisposing production of MPO-ANCA were designated *Man-1* and *Man-2*. To our knowledge, this is the first paper defining QTLs as susceptible for aberrant production of MPO-ANCA.

There were two SCG/Kj-derived pleiotropic QTLs on chromosome 1, *Scg-1* and *Scg-2*. *Scg-1* was linked to hyperproduction of IgG, anti-DNA Ab, antichromatin Ab, GN, crescent formation, vasculitis, splenomegaly, and shortened lifespan. It was mapped to the previously reported positions of *Sle1* (NZW derived; see Ref. 5), *Lbw7*, *Nba2* (NZB derived; see Refs. 15 and 16), and *Bxs3* (BXSB derived; see Ref. 17). Those QTLs are susceptible to various immunological traits, including antinuclear Ab production, splenomegaly, GN, and hypocomplementemia (5, 15, 16). This locus has been defined (18) for initial spontaneous loss of immunologic tolerance because of its wide variety of traits. One characteristic of *Scg-1* is that it was not associated with the total IgM level at a young (12 wk) or old (24 wk) age. This observation suggests that *Scg-1* influences not only activation but also differentiation of B cells. Candidate genes for the *Scg-1*-interval are *Tnfsf6*, *Cd3z*, and *Fcgr2b/3*. The Fas ligand encoded by *Tnfsf6* is a type II membrane protein on activated T cells and binds to Fas (19). The Fas ligand in *gld* mice carries a point mutation and causes lymphadenopathy and autoimmune diseases similar to those of MRL/*lpr* mice (20). *Cd3z* is the gene for the CD3 ζ-chain, the principal signal transduction element of the TCR (21). Abnormal expression of the TCR/CD3 complex on T cells in human SLE patients has been reported (22). Polymorphism(s) of all these genes possibly result in alteration of T cell function and survival of autoreactive lymphocytes. Fc receptors for IgG (FcγR) have important functions in the activation and down-modulation of immune responses. Balanced signaling through activating (FcγRIII) and inhibitory (FcγRIIb) FcγRs intimately regulates the activity of various cells in immune system (23, 24). There is evidence that reduced expression of inhibitory FcγR on B cells is observed in SLE-prone mouse strains (NZB, BXSB, SB/Le, and MRL) due to the polymorphic promoter regions of the *Fcgr2b* gene (10, 25). Moreover, expression of activating FcγRIII is abnormally high in SLE-prone mice such as MRL mice (25). Down-regulation of FcγRII on B cells affects the extent of IgG-class Ab response to T cell-dependent Ags (10). FcγRIIb-deficient $Fas^{lpr/lpr}$ is reported to be sufficient for the development of murine SLE even in a B_6 background (26). Single nucleotide polymorphisms of the *FCGR2B* gene associate with human SLE (27). Hence, *Fcgr2b* and *Fcgr3* are attractive candidate genes for autoimmunity in SCG/Kj mice.

The second SCG/Kj-inherited chromosome 1 locus, *Scg-2*, was linked to total IgG level, the production of IgG-class autoantibodies, GN, splenomegaly, and shortened lifespan. *Scg-2* is located in

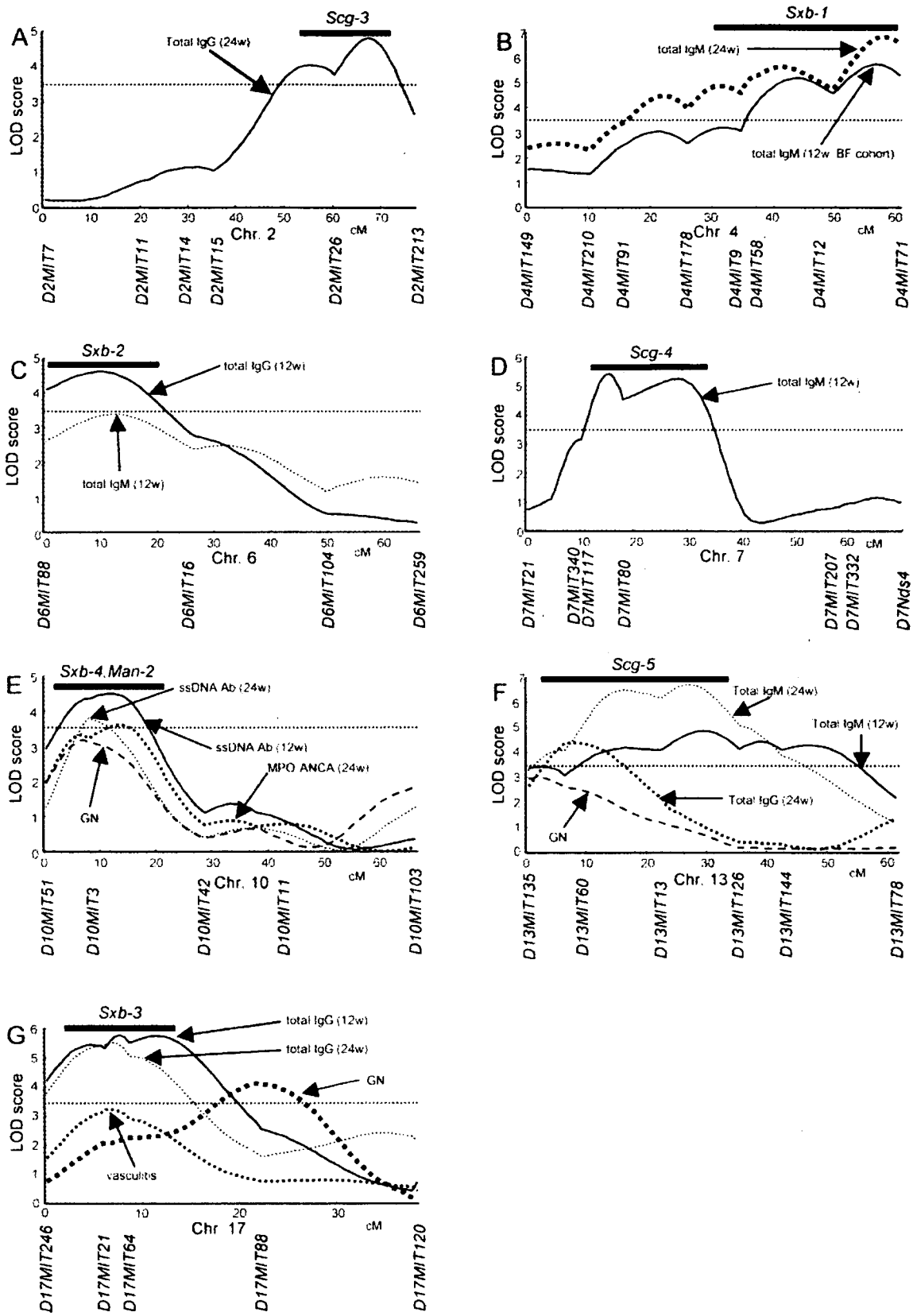

FIGURE 3. Interval mapping scans showing QTLs *Scg-1* to *Scg-5*, *Sxb-1* to *Sxb-4*, and *Man-2*. LOD score curves for each of quantitative traits in the cohort(s) of maximum log-likelihood value are shown (see Table IV). Dotted horizontal lines indicate significant LOD threshold values determined by permutation tests. A one-log support interval for each QTL is shown with a solid bar at the *top*. One-log support intervals and significant LOD threshold values for multiple traits were determined based on LOD values of total 24-wk (24w) IgG for *Scg-3* (*A*), total 12-wk (12w) IgM for *Sxb-1* (*B*), 12-wk total IgG for *Sxb-2* (*C*), 12-wk total IgM for *Scg-4* (*D*), 12-wk ssDNA Ab and 24-wk MPO-ANCA for *Sxb-4*/*Man-2* (*E*), 24-wk total IgM and IgG for *Scg-5* (*F*), and 24-wk total IgG for *Sxb-3* (*G*). Chr., chromosome.

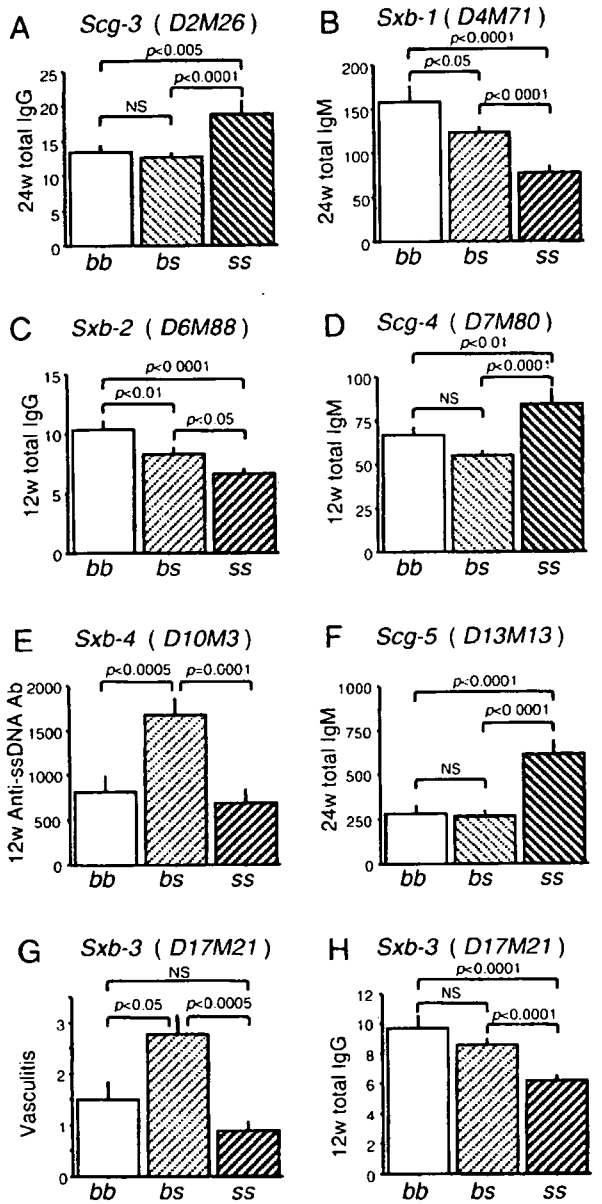

FIGURE 4. Differences in autoimmune phenotypes at each QTL. Names of QTLs and representative markers are shown at the *top* of each panel (*A–H*). Traits controlled by each QTL are shown on the left of the *y*-axis. *p* values in Fisher's protected least significant difference procedure are shown. NS, not significant.

the middle of chromosome 1 and is proximal to *Sbw1* (NZB derived; see Ref. 15), which is linked to splenomegaly, and *Bxs2* (BXSB derived; see Ref. 17), which is linked to GN and autoantibody production. *Scg-1* and *Scg-2* are ~25 cM apart and are likely to be two distinct genes, because their spectra of controlling traits and mode of inheritance were different. The most striking difference is that only *Scg-2* was linked to aberrant production of MPO-ANCA. This finding allows us to postulate that in the *Scg-2* interval are two different genes, one of which controls propagation and differentiation of lymphocyte; the other (*Man-1*) is related to granulocytes, the major origin of released MPO. Candidate genes for *Man-1* are *Daf1/2* and *Serpinb2*. *Daf1/2* are genes encoding decay-accelerating factor (DAF), a C3 convertase inhibitor preventing complement-mediated autologous attack. DAF deficiency in human is known as paroxysmal nocturnal hemoglobinuria, a disease of spontaneous hemolysis due to an uncontrolled complement system. Human neutrophils, as well as erythrocytes, express DAF on their surface, and the expression is doubled when activated (28, 29). The lysis of neutrophils from paroxysmal nocturnal hemoglobinuria patients is increased at least in vitro (30). Taken together, it is possible that polymorphism(s) of *Daf* genes result in the fragility of neutrophils, the increased release of MPO, and more opportunity for MPO to be presented as an autoantigen. *Serpinb2* is also an intriguing candidate. It is the gene encoding plasminogen activator inhibitor type 2 (PAI-2), a member of the serine proteinase inhibitor (serpin) genes that exhibit inhibition toward the urokinase-type plasminogen activator (31). PAI-2 is detected mainly in monocyte/macrophage and modulates their functions such as inhibition of apoptosis and altered expression of the adhesion molecule and DAF (31–33). Because neutrophils express PAI-2 as well as monocytes in the inflammatory state and contribute to the persistence of fibrin and localization of infection (34), these roles of PAI-2 in inflammation possibly result in a more efficient presentation of MPO as an autoantigen in this cytokine milieu.

Scg-3 (chromosome 2), *Scg-4* (chromosome 7), and *Scg–5* (chromosome 13) are SCG/Kj-derived QTLs and are linked not to autoantibody production but to elevated total Ig levels, suggesting their influence on polyclonal B cell activation. *Scg-3* on chromosome 2 may overlap with the MRL-derived QTL reported by Gu et al. (35). A possible candidate gene is *Il1*, because it can influence IgG production in human SLE (36). Several reports of murine QTLs for lupus are on proximal-mid chromosome 7: NZB-derived *Sle3* (5), *Lbw5* (15), *Nba5* (37), and MRL-derived *Lmb3* (38). The positional candidate gene for *Scg-4* is *Cd22*, a negative regulator for the BCR signal, and *Bax*, a proapoptotic protein expressed in lymphocytes. Both of these molecules are described as related to lupus (39, 40). Several authors (37, 41) have mapped QTLs as controlling the production of nephritogenic gp70 autoantigen and its immune complex on proximal-mid chromosome 13. Yoshiki et al. (42) reported that gp70 was related to the pathogenesis of the immune complex GN of New Zealand mice. *Scg-5* may represent these QTLs, because it is linked to GN and Ig production (Table IV and Fig. 3*F*), and both BXSB and MRL mice are strains of high gp70 production (43).

Sxb-1 (chromosome 4), *Sxb-2* (chromosome 6), *Sxb-3* (chromosome 17), and *Sxb-4* (chromosome 10) are B_6-derived QTLs and were linked to various traits, including hypergammaglobulinemia, autoantibody production, GN, and vasculitis. NZB-derived loci (*Sle2* (5), *Lbw2* (15) and *Nba1* (44)), BXSB-derived loci (*Acla-2* (45) and *Lxw1* (46)), and MRL-derived loci (*Arvm2* (47) and *Asm2* (48)) were previously mapped to chromosome 4. Of interest, *Lmb1* (38) is an additively inherited B_6-derived locus linked to lymphadenopathy and anti-DNA Ab production defined by using (MRL-*Fas*^{lpr} × B_6-*Fas*^{lpr}) F_2. *Sxb-1* and *Lmb1* share their mode of inheritance and maximal likelihood locations on chromosome 4. Thus, *Sxb-1* may represent some of these QTLs, especially *Lmb1*. Multiple candidate genes are to be considered, such as *Ifa*, *C1q*, and *Tnfr-2*. IFN-α can break tolerance and initiate autoimmunity under prolonged expression (49). C1q deficiency causes autoimmunity by impairment of the clearance of apoptotic cells (50). Polymorphism of TNFR type II is causative of augmented IL-6 production, and such a polymorphism is associated with human SLE (51). These findings suggest that *Ifa*, *C1q*, and *Tnfr-2* on chromosome 4 are possible candidates for *Sxb-1*. *Sxb-2* on chromosome 6 is linked to both IgM and IgG levels, suggesting harbored T cell-activating candidate(s) as well as B cell activators. *Tcrb* is within the *Sxb-2* interval and can be a candidate, because Vβ repertoire skewing of TCR is observed in both murine and human SLE (52,

53). *Sxb-3* is such a multifunctional QTL that mice of heterozygous alleles and/or mice homozygous for B_6 allele exhibit stronger traits than those of SCG/Kj homozygous alleles. The candidate gene for *Sxb-3* is H-2, the murine MHC. B_6, one of parental strains used in this study, carries the H-2^b haplotype. Because of a defect in the *Ea* gene, mice with the H-2^b haplotype do not express class II E molecules, the importance of which is shown in the SLE-prone BXSB strain carrying the H-2^b haplotype. The development of disease is more accelerated in BXSB.H-2^b mice than in BXSB.H-2^d mice (54). The transgene of E molecules in animals with H-$2^{k/b}$ lessens the disease phenotypes (55). These facts are consistent with the result that heterozygous H-$2^{b/k}$ and/or homozygous H-2^b mice exhibited more severe autoimmune phenotypes in our study.

Sxb-4 (*Man-2*) is also a multifunctional QTL, such that mice of the heterozygous genotype exhibit stronger traits than those with either homozygous genotype. This locus mapped centromeric to previously defined MRL-derived *Lmb4* (38) and *Asm1* (48) and is possibly distinct from these. Candidate genes for *Sxb-4* are *Ifngr1* and *Myb*; *Ifngr1* encodes IFN-γ receptor 1. The frequency of heterozygous amino acid polymorphism (V14M) of *IFNGR1* in human SLE patients is significantly higher than in the control population (56). c-*myb* expression and aberrant lymphocyte proliferation are associated in MRL/*lpr* mice (57). Each of these genes possibly contributes to the development of disease through abnormal lymphocyte proliferation or altered cytokine milieu.

The localization of disease-susceptibility genes in the murine model provides important information for the prediction of loci contributing to human disease, because linked genes on chromosomes are conserved between mice and humans. The further characterization of the disease susceptibility loci identified in this work will be helpful in focusing future human studies on specific syntenic intervals, leading to the definition of human susceptibility genes.

Acknowledgments

We thank Dr. Okio Hino, Department of Pathology, and Dr. Yasuhiko Tomino, Department of Nephrology, Juntendo University School of Medicine (Tokyo, Japan). We also thank N. Ohtsuji, M. Ohtsuji, K. Sasahara, and Dr. Y. Shida for their skillful technical assistance and Dr. Kyogoku for the use of the SCG/Kj mice.

Disclosures

The authors have no financial conflict of interest.

References

1. Kinjoh, K., M. Kyogoku, and R. A. Good. 1993. Genetic selection for crescent formation yields mouse strain with rapidly progressive glomerulonephritis and small vessel vasculitis. *Proc. Natl. Acad. Sci. USA* 90: 3413–3417.
2. Miyazawa, S., K. Saiga, K. Nemoto, T. Mae, and O. Hotta. 2002. A repeat biopsy study in spontaneous crescentic glomerulonephritis mice. *Ren. Fail.* 24: 557–566.
3. Jennette, J. C., and R. J. Falk. 1994. The pathology of vasculitis involving the kidney. *Am. J. Kidney Dis.* 24: 130–141.
4. Ishida-Okawara, A., T. Ito-Ihara, E. Muso, T. Ono, K. Saiga, K. Nemoto, and K. Suzuki. 2004. Neutrophil contribution to the crescentic glomerulonephritis in SCG/Kj mice. *Nephrol. Dial. Transplant.* 19: 1708–1715.
5. Morel, L., U. H. Rudofsky, J. A. Longmate, J. Schiffenbauer, and E. K. Wakeland. 1994. Polygenic control of susceptibility to murine systemic lupus erythematosus. *Immunity* 1: 219–229.
6. Wang, Y., M. Nose, T. Kamoto, M. Nishimura, and H. Hiai. 1997. Host modifier genes affect mouse autoimmunity induced by the lpr gene. *Am. J. Pathol.* 151: 1791–1798.
7. Kono, D. H., M. S. Park, and A. N. Theofilopoulos. 2003. Genetic complementation in female (BXSB × NZW) F_2 mice. *J. Immunol.* 171: 6442–6447.
8. Knight, J. G., D. D. Adams, and H. D. Purves. 1977. The genetic contribution of the NZB mouse to the renal disease of the NZB × NZW hybrid. *Clin. Exp. Immunol.* 28: 352–358.
9. Bates, D. L., P. J. Butler, E. C. Pearson, and J. O. Thomas. 1981. Stability of the higher order structure of chicken-erythrocyte chromatin in solution. *Eur. J. Biochem.* 119: 469–476.
10. Jiang, Y., S. Hirose, M. Abe, R. Sanokawa-Akakura, M. Ohtsuji, X. Mi, N. Li, Y. Xiu, D. Zhang, J. Shirai, et al. 2000. Polymorphisms in IgG Fc receptor IIB regulatory regions associated with autoimmune susceptibility. *Immunogenetics* 51: 429–435.
11. Churchill, G. A., and R. W. Doerge. 1994. Empirical threshold values for quantitative trait mapping. *Genetics* 138: 963–971.
12. Nose, M., M. Nishimura, and M. Kyogoku. 1989. Analysis of granulomatous arteritis in MRL/Mp autoimmune disease mice bearing lymphoproliferative genes: the use of mouse genetics to dissociate the development of arteritis and glomerulonephritis. *Am. J. Pathol.* 135: 271–280.
13. Hogarth, M. B., J. H. Slingsby, P. J. Allen, E. M. Thompson, P. Chandler, K. A. Davies, E. Simpson, B. J. Morley, and M. J. Walport. 1998. Multiple lupus susceptibility loci map to chromosome 1 in BXSB mice. *J. Immunol.* 161: 2753–2761.
14. Lander, E. S., and D. Botstein. 1989. Mapping Mendelian factors underlying quantitative traits using RFLP linkage maps. *Genetics* 121: 185–199.
15. Kono, D. H., R. W. Burlingame, D. G. Owens, A. Kuramochi, R. S. Balderas, D. Balomenos, and A. N. Theofilopoulos. 1994. Lupus susceptibility loci in New Zealand mice. *Proc. Natl. Acad. Sci. USA* 91: 10168–10172.
16. Vyse, T. J., S. J. Rozzo, C. G. Drake, S. Izui, and B. L. Kotzin. 1997. Control of multiple autoantibodies linked with a lupus nephritis susceptibility locus in New Zealand black mice. *J. Immunol.* 158: 5566–5574.
17. Haywood, M. E., M. B. Hogarth, J. H. Slingsby, S. J. Rose, P. J. Allen, E. M. Thompson, M. A. Maibaum, P. Chandler, K. A. Davies, E. Simpson, et al. 2000. Identification of intervals on chromosomes 1, 3, and 13 linked to the development of lupus in BXSB mice. *Arthritis Rheum.* 43: 349–355.
18. Morel, L., and E. K. Wakeland. 2000. Lessons from the NZM2410 model and related strains. *Int. Rev. Immunol.* 19: 423–446.
19. Suda, T., T. Takahashi, P. Golstein, and S. Nagata. 1993. Molecular cloning and expression of the Fas ligand, a novel member of the tumor necrosis factor family. *Cell* 75: 1169–1178.
20. Takahashi, T., M. Tanaka, C. I. Brannan, N. A. Jenkins, N. G. Copeland, T. Suda, and S. Nagata. 1994. Generalized lymphoproliferative disease in mice, caused by a point mutation in the Fas ligand. *Cell* 76: 969–976.
21. Irving, B. A., and A. Weiss. 1991. The cytoplasmic domain of the T cell receptor ζ-chain is sufficient to couple to receptor-associated signal transduction pathways. *Cell* 64: 891–901.
22. Tsuzaka, K., I. Fukuhara, Y. Setoyama, K. Yoshimoto, K. Suzuki, T. Abe, and T. Takeuchi. 2003. TCR ζ mRNA with an alternatively spliced 3′-untranslated region detected in systemic lupus erythematosus patients leads to the down-regulation of TCR zeta and TCR/CD3 complex. *J. Immunol.* 171: 2496–2503.
23. Ravetch, J. V., and S. Bolland. 2001. IgG Fc receptors. *Annu. Rev. Immunol.* 19: 275–290.
24. Takai, T. 2002. Roles of Fc receptors in autoimmunity. *Nat. Rev. Immunol.* 2: 580–592.
25. Pritchard, N. R., A. J. Cutler, S. Uribe, S. J. Chadban, B. J. Morley, and K. G. Smith. 2000. Autoimmune-prone mice share a promoter haplotype associated with reduced expression and function of the Fc receptor FcγRII. *Curr. Biol.* 10: 227–230.
26. Yajima, K., A. Nakamura, A. Sugahara, and T. Takai. 2003. FcγRIIB deficiency with Fas mutation is sufficient for the development of systemic autoimmune disease. *Eur. J. Immunol.* 33: 1020–1029.
27. Li, X., J. Wu, R. H. Carter, J. C. Edberg, K. Su, G. S. Cooper, and R. P. Kimberly. 2003. A novel polymorphism in the Fcγ receptor IIB (CD32B) transmembrane region alters receptor signaling. *Arthritis Rheum.* 48: 3242–3252.
28. Okuda, K., A. Kanamaru, E. Ueda, T. Kitani, and K. Nagai. 1990. Membrane expression of decay-accelerating factor on neutrophils from normal individuals and patients with paroxysmal nocturnal hemoglobinuria. *Blood* 75: 1186–1191.
29. Berger, M., and M. E. Medof. 1987. Increased expression of complement decay-accelerating factor during activation of human neutrophils. *J. Clin. Invest.* 79: 214–220.
30. Brubaker, L. H., L. J. Essig, and C. E. Mengel. 1977. Neutrophil lifespan in paroxysmal nocturnal hemoglobinuria. *Blood* 50: 657–662.
31. Yu, H., F. Maurer, and R. L. Medcalf. 2002. Plasminogen activator inhibitor type 2: a regulator of monocyte proliferation and differentiation. *Blood* 99: 2810–2818.
32. Gan, H., G. W. Newman, and H. G. Remold. 1995. Plasminogen activator inhibitor type 2 prevents programmed cell death of human macrophages infected with *Mycobacterium avium*, serovar 4. *J. Immunol.* 155: 1304–1315.
33. Costelloe, E. O., K. J. Stacey, T. M. Antalis, and D. A. Hume. 1999. Regulation of the plasminogen activator inhibitor-2 (PAI-2) gene in murine macrophages: demonstration of a novel pattern of responsiveness to bacterial endotoxin. *J. Leukocyte Biol.* 66: 172–182.
34. Haj, M. A., L. A. Robbie, G. D. Adey, and B. Bennett. 1995. Inhibitors of plasminogen activator in neutrophils and mononuclear cells from septic patients. *Thromb. Haemost.* 74: 1528–1532.
35. Gu, L., A. Weinreb, X. P. Wang, D. J. Zack, J. H. Qiao, R. Weisbart, and A. J. Lusis. 1998. Genetic determinants of autoimmune disease and coronary vasculitis in the MRL-*lpr/lpr* mouse model of systemic lupus erythematosus. *J. Immunol.* 161: 6999–7006.
36. Jandl, R. C., J. L. George, C. A. Dinarello, and P. H. Schur. 1987. The effect of interleukin 1 on IgG synthesis in systemic lupus erythematosus. *Clin. Immunol. Immunopathol.* 45: 384–394.
37. Kikuchi, S., L. Fossati-Jimack, T. Moll, H. Amano, E. Amano, A. Ida, N. Ibnou-Zekri, C. Laporte, M. L. Santiago-Raber, S. J. Rozzo, et al. 2005. Differential role of three major New Zealand Black-derived loci linked with *Yaa*-induced murine lupus nephritis. *J. Immunol.* 174: 1111–1117.

38. Vidal, S., D. H. Kono, and A. N. Theofilopoulos. 1998. Loci predisposing to autoimmunity in MRL-Fas^{lpr} and C57BL/6-Fas^{lpr} mice. *J. Clin. Invest.* 101: 696–702.
39. Lajaunias, F., A. Ida, S. Kikuchi, L. Fossati-Jimack, E. Martinez-Soria, T. Moll, C. L. Law, and S. Izui. 2003. Differential control of CD22 ligand expression on B and T lymphocytes, and enhanced expression in murine systemic lupus. *Arthritis Rheum.* 48: 1612–1621.
40. Nazareth, M., P. Fanti, C. Schwach, K. Poppenberg, K. Janis, and S. M. Aronica. 2001. Altered Bax expression and decreased apoptosis in bone marrow cells of lupus-susceptible NZB/W mice. *Lupus* 10: 785–793.
41. Haywood, M. E., T. J. Vyse, A. McDermott, E. M. Thompson, A. Ida, M. J. Walport, S. Izui, and B. J. Morley. 2001. Autoantigen glycoprotein 70 expression is regulated by a single locus, which acts as a checkpoint for pathogenic anti-glycoprotein 70 autoantibody production and hence for the corresponding development of severe nephritis, in lupus-prone BXSB mice. *J. Immunol.* 167: 1728–1733.
42. Yoshiki, T., R. C. Mellors, M. Strand, and J. T. August. 1974. The viral envelope glycoprotein of murine leukemia virus and the pathogenesis of immune complex glomerulonephritis of New Zealand mice. *J. Exp. Med.* 140: 1011–1027.
43. Hara, I., S. Izui, P. J. McConahey, J. H. Elder, F. C. Jensen, and F. J. Dixon. 1981. Induction of high serum levels of retroviral env gene products (gp70) in mice by bacterial lipopolysaccharide. *Proc. Natl. Acad. Sci. USA* 78: 4397–4401.
44. Drake, C. G., S. K. Babcock, E. Palmer, and B. L. Kotzin. 1994. Genetic analysis of the NZB contribution to lupus-like autoimmune disease in (NZB × NZW)F1 mice. *Proc. Natl. Acad. Sci. USA* 91: 4062–4066.
45. Ida, A., S. Hirose, Y. Hamano, S. Kodera, Y. Jiang, M. Abe, D. Zhang, H. Nishimura, and T. Shirai. 1998. Multigenic control of lupus-associated antiphospholipid syndrome in a model of (NZW × BXSB) F_1 mice. *Eur. J. Immunol.* 28: 2694–2703.
46. Kono, D. H., M. S. Park, and A. N. Theofilopoulos. 2003. Genetic complementation in female (BXSB × NZW)F2 mice. *J. Immunol.* 171: 6442–6447.
47. Qu, W. M., T. Miyazaki, M. Terada, L. M. Lu, M. Nishihara, A. Yamada, S. Mori, Y. Nakamura, H. Ogasawara, C. Yazawa, et al. 2000. Genetic dissection of vasculitis in MRL/lpr lupus mice: a novel susceptibility locus involving the *CD72c* allele. *Eur. J. Immunol.* 30: 2027–2037.
48. Nishihara, M., M. Terada, J. Kamogawa, Y. Ohashi, S. Mori, S. Nakatsuru, Y. Nakamura, and M. Nose. 1999. Genetic basis of autoimmune sialadenitis in MRL/lpr lupus-prone mice: additive and hierarchical properties of polygenic inheritance. *Arthritis Rheum.* 42: 2616–2623.
49. Ronnblom, L., M. L. Eloranta, and G. V. Alm. 2003. Role of natural interferon-α producing cells (plasmacytoid dendritic cells) in autoimmunity. *Autoimmunity* 36: 463–472.
50. Botto, M., C. Dell'Agnola, A. E. Bygrave, E. M. Thompson, H. T. Cook, F. Petry, M. Loos, P. P. Pandolfi, and M. J. Walport. 1998. Homozygous C1q deficiency causes glomerulonephritis associated with multiple apoptotic bodies. *Nat. Genet.* 19: 56–59.
51. Morita, C., T. Horiuchi, H. Tsukamoto, N. Hatta, Y. Kikuchi, Y. Arinobu, T. Otsuka, T. Sawabe, S. Harashima, K. Nagasawa, and Y. Niho. 2001. Association of tumor necrosis factor receptor type II polymorphism 196R with systemic lupus erythematosus in the Japanese: molecular and functional analysis. *Arthritis Rheum.* 44: 2819–2827.
52. Sutmuller, M., H. J. Baelde, S. Ouellette, E. De Heer, and J. A. Bruijn. 1998. T-cell receptor Vβ gene expression in experimental lupus nephritis. *Immunology* 95: 18–25.
53. Massengill, S. F., M. M. Goodenow, and J. W. Sleasman. 1998. SLE nephritis is associated with an oligoclonal expansion of intrarenal T cells. *Am. J. Kidney Dis.* 31: 418–426.
54. Merino, R., L. Fossati, M. Lacour, R. Lemoine, M. Higaki, and S. Izui. 1992. H-2-linked control of the *Yaa* gene-induced acceleration of lupus-like autoimmune disease in BXSB mice. *Eur. J. Immunol.* 22: 295–299.
55. Iwamoto, M., N. Ibnou-Zekri, K. Araki, and S. Izui. 1996. Prevention of murine lupus by an I-E α-chain transgene: protective role of I-E α-chain-derived peptides with a high affinity to I-A^b molecules. *Eur. J. Immunol.* 26: 307–314.
56. Nakashima, H., H. Inoue, M. Akahoshi, Y. Tanaka, K. Yamaoka, E. Ogami, S. Nagano, Y. Arinobu, H. Niiro, T. Otsuka, and Y. Niho. 1999. The combination of polymorphisms within interferon-γ receptor 1 and receptor 2 associated with the risk of systemic lupus erythematosus. *FEBS Lett.* 453: 187–190.
57. Mountz, J. D., and A. D. Steinberg. 1989. Studies of c-*myb* gene regulation in MRL-*lpr/lpr* mice: Identification of a 5′ c-*myb* nuclear protein binding site and high levels of binding factors in nuclear extracts of *lpr/lpr* lymph node cells. *J. Immunol.* 142: 328–335.

JOURNAL OF VIROLOGY, June 2007, p. 5940–5948 Vol. 81, No. 11
0022-538X/07/$08.00+0 doi:10.1128/JVI.02137-06

Downregulation of an Astrocyte-Derived Inflammatory Protein, S100B, Reduces Vascular Inflammatory Responses in Brains Persistently Infected with Borna Disease Virus▽

Naohiro Ohtaki,[1] Wataru Kamitani,[1]† Yohei Watanabe,[1] Yohei Hayashi,[1] Hideyuki Yanai,[1] Kazuyoshi Ikuta,[1] and Keizo Tomonaga[1,2]*

Department of Virology, Research Institute for Microbial Diseases (BIKEN), Osaka University, Suita, Osaka 565-0871, Japan,[1] and PRESTO, Japan Science and Technology Agency, Kawaguchi, Saitama 332-0012, Japan[2]

Received 29 September 2006/Accepted 16 March 2007

Borna disease virus (BDV) is a neurotropic virus that causes a persistent infection in the central nervous system (CNS) of many vertebrate species. Although a severe reactive gliosis is observed in experimentally BDV-infected rat brains, little is known about the glial reactions contributing to the viral persistence and immune modulation in the CNS. In this regard, we examined the expression of an astrocyte-derived factor, S100B, in the brains of Lewis rats persistently infected with BDV. S100B is a Ca^{2+}-binding protein produced mainly by astrocytes. A prominent role of this protein appears to be the promotion of vascular inflammatory responses through interaction with the receptor for advanced glycation end products (RAGE). Here we show that the expression of S100B is significantly reduced in BDV-infected brains despite severe astrocytosis with increased glial fibrillary acidic protein immunoreactivity. Interestingly, no upregulation of the expression of S100B, or RAGE, was observed in the persistently infected brains even when incited with several inflammatory stimuli, including lipopolysaccharide. In addition, expression of the vascular cell adhesion molecule 1 (VCAM-1), as well as the infiltration of encephalitogenic T cells, was significantly reduced in persistently infected brains in which an experimental autoimmune encephalomyelitis was induced by immunization with myelin-basic protein. Furthermore, we demonstrated that the continuous activation of S100B in the brain may be necessary for the progression of vascular immune responses in neonatally infected rat brains. Our results suggested that BDV infection may impair astrocyte functions via a downregulation of S100B expression, leading to the maintenance of a persistent infection.

Astrocytes are activated in response to damage to the central nervous system (CNS) caused by ischemia, trauma, neurodegenerative disorders, autoimmunity, and infectious diseases (35). The process by which reactive astrocytes are recruited to the injured CNS remains rather obscure, but astrocytosis is postulated to play an important role in the maintenance of homeostasis in the CNS (5). Reactive astrocytes show higher levels of adhesion molecules and also increase the production of a variety of cytokines, chemokines, growth factors, and neuropeptides (35), consequently eliciting a brain inflammatory response. Although the modulation of CNS-based immune responses followed by astrocytosis seems to be engaged in negative effects on the injured brain, reactive astrocytes are nevertheless essential for the repair of damage to immune-privileged organs attacked by pathogens (5, 7, 35).

Infections by neurotropic viruses generally reactivate glial cells in infected brains. Borna disease virus (BDV) is a highly neurotropic virus that causes severe neurological disorders in many vertebrate species (18, 38). Like many pathogens targeting the CNS, BDV strongly induces glial reactivation in the brains of experimentally infected animals (16, 39, 50). BDV characteristically establishes a persistent infection without any cytopathic effects in brain cells (8, 12, 14, 39), and so studies of this virus provide a good understanding of the modulation of the brain immune response during the persistence of CNS pathologies. Numerous studies have demonstrated that persistent infections of BDV induce a chronic astrocytosis, as well as a stable upregulation of the expression of proinflammatory cytokines, such as interleukin 1-beta (IL-1β) and tumor necrosis factor alpha (TNF-α), in the brain (16, 31, 39). Despite such lasting inflammatory responses, this virus efficiently maintains the infection and has a life-long survival in the CNS. At present, modulation of the immune responses, such as Th1-specific T-cell tolerance, has been proposed as the mechanism for the maintenance of BDV persistence in mice (8, 12, 14). Although reactive astrocytes appear to be involved in the homeostatic preservation of infected brains, little is known about the glial reactions contributing to the persistence of CNS pathologies or to the regulation of the inflammatory responses in damaged brains.

In this study, we examined the expression of an astrocyte-derived factor, S100B, in rats persistently infected with BDV to understand the glial reactions occurring during a chronic viral infection. S100B is an EF-hand Ca^{2+}-binding protein produced mainly by astrocytes that exerts autocrine and paracrine effects on neural cells, stimulating cellular survival, proliferation, and differentiation (1, 3, 6, 32, 40). A prominent role of this protein appears to be the promotion of inflammatory re-

* Corresponding author. Mailing address: Department of Virology, Research Institute for Microbial Diseases, Osaka University, 3-1 Yamadaoka, Suita Osaka 565-0871, Japan. Phone: 81-6-6879-8308. Fax: 81-6-6879-8310. E-mail: tomonaga@biken.osaka-u.ac.jp.

† Present address: Department of Microbiology and Immunology, University of Texas Medical Branch at Galveston, 301 University Blvd., MRB 4.162, Galveston, TX 77555-1019.

▽ Published ahead of print on 21 March 2007.

sponses, as a cytokine, through binding to its cellular surface receptor, the receptor for advanced glycation end products (RAGE) (36, 37, 51). Here we demonstrate that the expression of S100B is significantly reduced in persistently infected brains despite severe astrocytosis with increased glial fibrillary acidic protein (GFAP) immunoreactivity. Interestingly, no upregulation of the expression of S100B, or RAGE, was found in the brains of persistently infected rats exposed to a bacterial lipopolysaccharide (LPS) and immunized with myelin-basic protein (MBP), suggesting the possibility of a constitutive downmodulation of S100B in the persistently infected brains. Furthermore, expression of the vascular cell adhesion molecule 1 (VCAM-1) in the vascular endothelium and the subsequent vasodilatation were downregulated in the infected rat brains sensitized with MBP. We also showed that S100B signaling may be necessary for the development of mononuclear cell infiltrates via the activation of vascular immune responses in neonatally infected rat brains. Our findings may provide a novel mechanism by which chronic viral infections abrogate vascular inflammatory responses through the downregulation of an astrocyte-derived cytokine, S100B, leading to a persistent infection.

MATERIALS AND METHODS

Preparation and inoculation of the virus. A viral stock was prepared from the homogenate of rat brains infected with BDV strain huP2br (25), and the titer of the BDV source was measured as described previously (49). Briefly, semiconfluent monolayers of C6 cells were inoculated with serial 10-fold dilutions of the cell-free BDV stock. Three days after the inoculation, the cells were fixed with 4% paraformaldehyde and subjected to immunofluorescence staining. The viral titer was calculated as focus-forming units (FFU) per milliliter of cell-free BDV stock.

For viral infection, Lewis rats (SLC, Shizuoka, Japan) within 24 h after birth (neonate) and at 4 weeks old (adult) were intracranially inoculated in the left-brain hemisphere with 2,000 and 20,000 FFU of BDV stock per animal, respectively.

Administration of LPS. BDV-infected and uninfected rats were injected intraperitoneally with 200 or 500 μg/kg of LPS (*Escherichia coli* strain O111:B4; Sigma-Aldrich, St. Louis, MO) at 5 weeks postinfection (p.i.). The rats were sacrificed at 24, 48, and 72 h after the injection. As age-matched controls, animals were injected with phosphate-buffered saline (PBS) and sacrificed at 72 h after the administration.

Induction and clinical evaluation of experimental autoimmune encephalomyelitis. Experimental autoimmune encephalomyelitis (EAE) was induced in at least seven Lewis rats in each BDV-infected and uninfected group by subcutaneously injecting 100 μg of MBP (Sigma-Aldrich) in the lateral left upper leg. The injected emulsion contained 2 mg of MBP in 1 ml of PBS mixed with 1 ml of complete Freund's adjuvant (Wako Junyaku, Osaka, Japan). For immunohistochemical (IHC) analysis, animals were sacrificed at 14 days after the sensitization, at which time the clinical symptoms of EAE reached a peak in the uninfected controls. Animals were scored daily for clinical signs of disease on a severity scale ranging from 0 to 6 (where 0, normal; 1, limp tail; 2, hind limb weakness; 3, unilateral hind limb paralysis; 4, bilateral hind limb paralysis; 5, bilateral hind limb paralysis and incontinence; and 6, moribund). The results are presented as the mean daily clinical score of each experimental group.

Inoculation of recombinant BDV nucleoprotein antigen. The recombinant BDV nucleoprotein (N) protein was produced as reported previously (48). Briefly, the cDNA encoding BDV N was inserted into the plasmid pGEX, and the recombinant protein was expressed in *E. coli* as a fusion construct with glutathione *S*-transferase (GST) and then purified by using glutathione Sepharose 4B. The purified protein was cleaved by factor Xa to remove the GST, and the endotoxin in the protein solution was removed by a polymyxin B-coupled matrix (Bio-Rad Laboratories Inc., Hercules, CA). The recombinant N (rN) was analyzed using sodium dodecyl sulfate-polyacrylamide gel electrophoresis (SDS-PAGE). For sensitization, 50 μg of BDV rN was injected into rats at 3 weeks after the inoculation of BDV.

Inoculation with the soluble form of RAGE. To block S100B signaling, a soluble form of RAGE (RAGE-Fc; R&D Systems Inc., Minneapolis, MN), which is a recombinant, truncated form of rat RAGE spanning the extracellular domain and serving as a decoy (34), was employed. Rats received 100 μg/kg of RAGE-Fc at 2-day intervals by intraperitoneal (i.p.) injection, starting from the day of immunization with the rN.

Immunoblotting analysis. Brain extracts of Lewis rats were prepared by sonication in lysis buffer (1% NP-40, 50 mM Tris-HCl [pH 7.5], 1 mM EDTA, 100 mM NaCl) with a protease inhibitor cocktail (Nacalai Tesque, Inc., Kyoto, Japan). The aliquots were resolved in SDS-PAGE sample buffer. Equal amounts of total protein were subjected to 12% SDS-PAGE and transferred onto polyvinylidene difluoride membranes (Millipore, Bedford, MA). The membranes were blocked with 5% skimmed milk in PBS-0.1% Tween 20. The membranes were reacted with antibody against RAGE (1:100; Santa Cruz Biotechnology Inc., Santa Cruz, CA), HMGB1 (20) (1:1,000), tubulin (1:4,000; Sigma-Aldrich) at room temperature, or S100B (1:2,000; BD Bioscience, San Jose, CA) at 4°C. After being washed, the membranes were incubated with horseradish peroxidase-conjugated secondary antibodies (Jackson Immunoresearch Laboratories, West Grove, PA) for 1 h at 37°C. Reacted proteins on the membrane were then visualized using an ECL system Western blotting kit (Amersham Pharmacia Biotech, Uppsala, Sweden). The intensity of each band was quantified using NIH image software.

Histological and immunohistochemical analyses. Rat brains were fixed in 4% paraformaldehyde in PBS and embedded in paraffin. Deparaffinized sections (5 μm) were stained with hematoxylin and eosin (H&E). For IHC analysis, thin sections (4 μm) were incubated with a trypsin solution (0.1% trypsin, 0.1% $CaCl_2$, and 0.05 M Tris-HCl [pH 7.6]) for 15 min at 37°C. Endogenous peroxide was quenched with 0.5% HIO_4. After a blocking step, the sections were incubated with anti-GFAP mouse antibody (1:1,000; Lab Vision, Fremont, CA), anti-GFAP rabbit antibody (1:1,000; Chemicon, Temecula, CA), anti-rat CD68 (ED-1) (1:100; Serotec Ltd., Kidlington, Oxford, United Kingdom), anti-CD4 (1:100; Serotec Ltd.), anti-VCAM-1 (1:200; BD Bioscience), anti-RAGE (1:1,000) and/or anti-S100B (1:2,000; BD Bioscience) antibodies. After several washes, primary antibodies were detected by incubation with a biotinylated goat anti-biotin peroxidase complex (1:200; Vector, Burlingame, CA). Thereafter, the sections were incubated with the avidin-biotin peroxidase complex (1:125; Vector). Specific reactions were visualized with 3′,3′-diaminobenzidine-tetrahydrochloride (DAB). For immunofluorescence analysis, fluorescein-conjugated streptavidin (Vector) was used instead of an ABC kit. Alexa Fluor 555-conjugated secondary antibodies (Invitrogen, San Diego, CA) and 4′,6′-diamidino-2-phenylindole (DAPI) were used for counterstaining. Terminal deoxynucleotidyltransferase-mediated dUTP nick end labeling (TUNEL) was performed using an in situ cell death detection kit (Roche Molecular Diagnostics, Pleasanton, CA). For IHC analysis, polyclonal antibodies to human RAGE were generated by immunization of a rabbit with recombinant RAGE peptide (amino acids 102 to 346) expressed by *E. coli*.

Quantification of VCAM-1 expression in rat brains. For a quantitative analysis of VCAM-1 levels in the brain, an image of the area of interest was captured using a Nikon E600 microscope and charge-coupled device camera (Hamamatsu Photonics Inc., Hamamatsu, Japan) under the same optical and lighting conditions. The average of the optical densities of positive signals was measured in four different fields of the cerebellum in each section for four animals by using Photoshop and NIH image software. Using the software, the pixel intensity of DAB staining was extracted above the threshold to determine the optical density.

Semiquantitative reverse transcription-PCR for chemokine expression. Total RNA was extracted from rat brain homogenates by using the RNA isolation reagent TRIzol (Invitrogen). First-strand cDNAs were synthesized from aliquots of 2 μg of total RNA by a Thermoscript reverse transcription (RT)-PCR system (Invitrogen). The PCR primers used were as follows: macrophage-inflammatory protein 1β-sense (MIP-1β-sense) (5′-ATG AAG CTC TGC GTG TCT GCC TTC-3′); MIP-1β-antisense (5′-TCA GTT CAA CTC CAA GTC ATT CAC-3′); monocytes chemoattractant protein 1-sense (MCP-1-sense) (5′-ATG CAG GTC TCT GTC ACG CTT CTG GGC-3′); MCP-1-antisense (5′-CTA GTT CTC TGT CAT ACT GGT CAC-3′); glyceraldehyde-3-phosphate dehydrogenase sense (GAPDH-sense) (5′-ACC ACA GTC CAT GCC ATC AC-3′); and GAPDH-antisense (5′-TCC ACC ACC CTG TTG CTG TA-3′). PCR was performed in a total volume of 25 μl containing 1 μl of cDNA and 2 U of *Taq* polymerase (TaKaRa ExTaq; Takara Bio Inc., Shiga, Japan). The PCR was performed at 94°C for 30 s, at the annealing temperature for 30s, and at 72°C for 30s. The optimal number of amplification cycles and annealing temperature were changed for each primer.

Quantification of proinflammatory cytokines in rat brain. Estimations of the expression levels of the proinflammatory cytokines IL-1β and TNF-α in BDV-

infected rat brains were performed by using enzyme-linked immunosorbent assay (ELISA) kits (R&D Systems, Inc.), following the manufacturer's directions. Plates were analyzed at 492 nm, and levels of IL-1β and TNF-α were determined by comparison to a standard curve. The data were normalized to the amount of total protein used for the analysis.

Statistical analysis. Data were expressed as means ± standard error of the means. Statistical analyses were performed using an unpaired Student's *t* test or one-way analysis of variance followed by post hoc Dunnett's test compared with the control group. An *n* of 4 was used for each treatment group in statistical analyses, except for the indication.

RESULTS

Reduced expression of S100B, but not GFAP, in persistently infected rat brains. To understand the environment in the CNS during a persistent infection of BDV, neonatal BDV-infected (NBI) or 4-week-old adult BDV-infected (ABI) Lewis rats were sacrificed at 5 weeks p.i. As shown in numerous studies (21, 39), no significant immune cell infiltration was observed in NBI rats, whereas ABI rats showed a slight encephalitis with perivascular mononuclear cell infiltrates. Furthermore, a marked astrocytosis, as well as microgliosis, was observed in both NBI and ABI rat brains at 5 weeks p.i. and was present during the persistent stage of BDV infection in the rats (data not shown).

S100B is a Ca^{2+}-binding protein produced mainly by astrocytes in the CNS (35, 37). The expression level of S100B is most likely to be correlated with brain injuries, as well as the degree of astrocytosis (37, 44, 51), suggesting that the expression level may be a biomarker for the activity of astrocytes in inflamed brains. We therefore monitored the expression of S100B in rat brains persistently infected with BDV, in addition to the expression of GFAP, which is also specific to astrocytes. The immunoreaction of S100B is found mainly in the GFAP-positive astrocytes in the rat brain (Fig. 1A). In both NBI and ABI rat brains, a marked increase of GFAP staining was demonstrated at 5 weeks p.i. (Fig. 1B). In contrast, immunoreactivity of S100B appeared to be weaker in the persistently infected brains than uninfected brains in both the cerebral cortex and cerebellum (Fig. 1B). We estimated GFAP and S100B levels by Western immunoblotting at 5 weeks p.i. As shown in Fig. 1C, although persistent infections induced an upregulation of GFAP expression in association with the astrocytosis, interestingly, the expression of S100B was significantly reduced at 5 weeks p.i. in both NBI and ABI rat brains.

No upregulation of S100B or RAGE expression in the brains of persistently infected rats administered LPS. To understand whether the expression of S100B is constitutively reduced in the persistently infected brain, we intraperitoneally injected LPS into NBI rats at 5 weeks p.i., following previous studies demonstrating that the i.p. injection of LPS rapidly induces the release of proinflammatory cytokines, such as IL-1β and TNF-α, in the brain and subsequently upregulates the expression of S100B (19, 43). We used NBI rats in the subsequent experiments, since the expression of S100B represents an intense increase in the brains from the second postnatal week onward (45), suggesting that it could be difficult to detect the upregulated level of S100B by additional inflammatory stimuli in ABI rat brains. In addition, the inflammatory responses by the stimuli could be easy to detect in the NBI rat brains in which the background infiltrations developed by the initial infection are lacking. On the injection of LPS, the expression

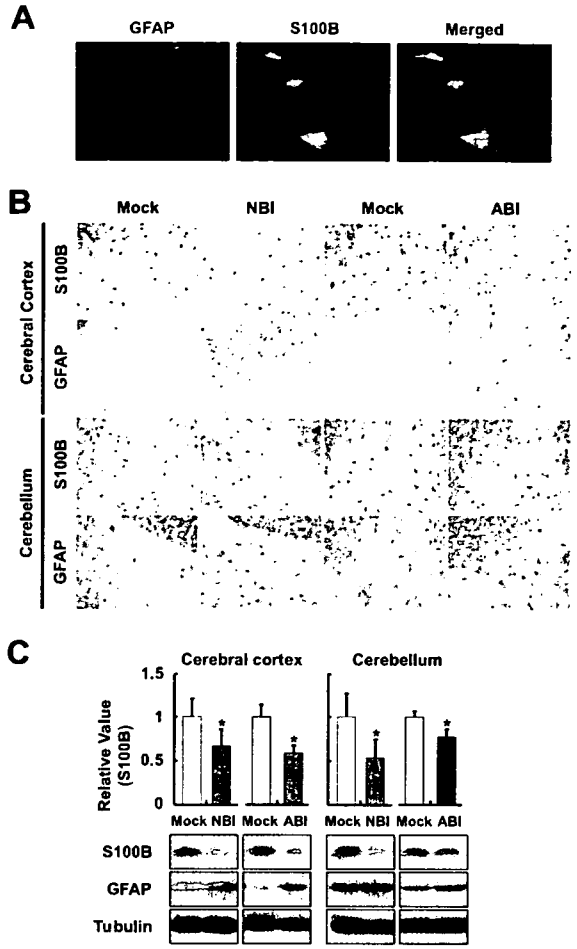

FIG. 1. Downregulation of S100B expression in BDV persistently infected brain. (A) S100B expression in BDV persistently infected Lewis rat brain. The cerebellum regions of NBI rats were stained with anti-GFAP (red) and anti-S100B (green) antibodies at 5 weeks p.i. The overlap in the distribution of GFAP and S100B is revealed in the merged image. The immunoreaction of S100B is found mainly in the GFAP-positive astrocytes. (B) Expressions of GFAP and S100B were detected in the cerebral cortex and cerebellum persistently infected with BDV. Brain sections from NBI and ABI rats at 5 weeks p.i. were immunostained with anti-GFAP and anti-S100B antibodies. Magnification, ×200. Mock, age-matched mock-infected rats. (C) Expression of S100B and GFAP proteins. The brain homogenates were obtained from the cerebral cortex and cerebellum regions of rat brains at 5 weeks p.i. and subjected to immunoblotting. The quantitative analysis of S100B expression is also shown. The band intensities were determined by NIH image. An *n* of 6 and *n* of 3 were used for the statistical analyses of NBI and ABI rats, respectively. Values were normalized to the tubulin level (⋆, $P < 0.05$ with mock-infected age-matched control rats).

of IL-1β was induced in both infected and uninfected rat brains, although it was expressed more so in the NBI than in mock-infected rats (Fig. 2A). In contrast, the expression of S100B was slightly reduced in the cerebellum of NBI rats at 48 h after the injection of LPS, while it was significantly increased in the uninfected rats (Fig. 2B). To confirm the distinct reactivation of S100B in the brain, we performed an IHC analysis using antibodies against the glial antigen. Consistent with the immunoblotting results, no upregulation of S100B

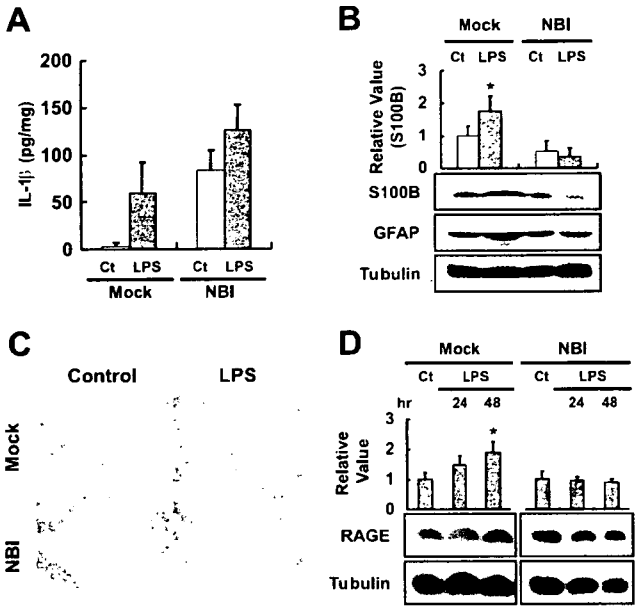

FIG. 2. LPS administration does not induce S100B expression in persistently infected brain. LPS was intraperitoneally administrated to BDV-infected rats at 5 weeks p.i., and the brains were collected 24 or 48 h after the injection. (A) Induction of IL-1β expression in LPS-injected bat brains. Amounts of IL-1β were measured with an ELISA kit. Ct, PBS-injected control rats; Mock, age-matched mock-infected rats. An n of 3 was used for the statistical analyses. (B) Expressions of S100B and GFAP were detected by immunoblotting. The brain homogenates were obtained from the cerebellum regions at 48 h after LPS injection. The quantitative analysis of S100B expression is also shown. The band intensities were determined by NIH image. Values were normalized to the tubulin level (*, $P < 0.05$ with PBS-injected control [Ct] rats). (C) Immunohistological analysis of S100B expression in the cerebellum regions of LPS- or PBS-treated (Control) rats. Magnification, ×200. Mock, age-matched mock-infected rats. (D) RAGE expression in LSP-injected animal brains. The quantitative analysis of RAGE expression is also shown. The band intensities were determined by NIH image. Values were normalized to the tubulin level. (*, $P < 0.05$ with PBS-injected control [Ct] rats).

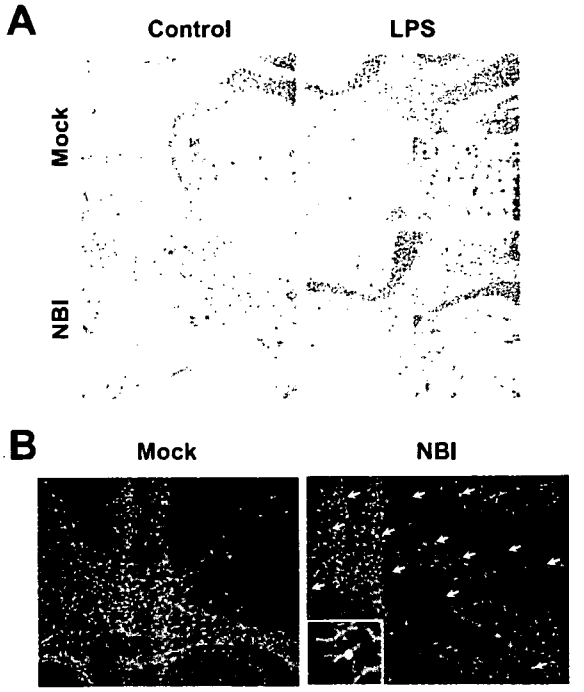

FIG. 3. Induction of neural apoptosis in LPS-injected persistently infected rat brains. (A) Immunohistological analysis of GFAP expression in the cerebellum regions of LPS- or vehicle-treated (Control) rats. Brain sections were obtained at 48 h after the injection and stained with anti-GFAP antibody. Magnification, ×200 (insets magnification, ×1,000). (B) TUNEL staining of LPS-treated NBI and mock-infected rats. Cerebellar areas at 48 h postinjection are shown. Arrows indicate apoptotic cells (green). GFAP-positive cells are shown in red. Counterstaining was done with DAPI (blue) for nuclear staining. Magnification, ×100 (insets magnification, ×1,000). Mock, age-matched mock-infected rats. An apoptosis-induced GFAP-positive glial cell is shown in the inset.

expression was observed in the cerebellum of LPS-injected NBI rats; rather, levels appeared to be slightly reduced in the infected brains (Fig. 2C).

That there was no upregulation of the expression of S100B in persistently infected brains suggested that the amount of this protein that is secreted may also be reduced in the CNS. To examine the secretion of S100B in the brain, we investigated the induction level of an S100B receptor, RAGE, in BDV-infected rat brains, because the expression of RAGE is upregulated by the direct interaction of S100B with RAGE (51). On the administration of LPS, the expression of RAGE was significantly upregulated in the cerebellum of uninfected rats by 48 h postinjection, whereas no expression of RAGE was induced in the persistently infected brains (Fig. 2D). It is worth noting that the expression of an alternative RAGE ligand, HMGB1, was upregulated in both infected and uninfected rat brains by LPS (data not shown), indicating that the unresponsiveness of RAGE expression is likely to be correlated with the decrease in the secretion of S100B in the infected brain.

Reduced stress resistance of brain cells in persistently infected NBI rats. The downregulation of S100B and RAGE expression suggested that the functions of S100B may be impaired in the NBI brains. Thus, we examined the vulnerability of neural cells under stressful environment conditions because previous reports demonstrated that S100B expression prevents neural cell apoptosis at an appropriate concentration via interaction with RAGE (17). In this regard, we estimated apoptotic cell death in the LPS-injected NBI rat brains, which show a decrease in the level of both S100B and RAGE reactivities (Fig. 2). The administration of LPS is known to upregulate production of nitric oxide in the brain, showing that LPS contributes to the development of a stressful environment within the CNS (42). We observed the immunoreactivity of GFAP, as well as conducted TUNEL staining. As shown in Fig. 3A, the reaction level of GFAP seems to be slightly reduced by the injection of LPS in BDV-infected brains at 48 h after the injection, although uninfected rats exhibited significantly enhanced GFAP expression in the brain. The immunoblot data also verified the reduced expression of GFAP in the NBI cerebellum (see Fig. 2B), suggesting that the number of astrocytes may decrease in the infected brain on the injection of LPS. In addition, the largest numbers of TUNEL-positive cells were found in the LPS-injected NBI rats at 5 weeks p.i., whereas the uninfected rat brains rarely contained positive cells (Fig. 3B). The TUNEL-positive cell population in the NBI brains contained both GFAP-